Cement and Concrete Research 129 (2020) 105959

Contents lists available at ScienceDirect

Cement and Concrete Research

journal homepage: www.elsevier.com/locate/cemconres

Investigation on the microstructure-related characteristics to elucidate performance of composite cement with limestone-calcined clay combination

Yuvaraj Dhandapani, Manu Santhanam*

Department of Civil Engineering, IIT Madras, India

ARTICLE INFO

Keywords:
composite cement blends
pore structure
tortuosity
chloride resistance
microstructure
capillary porosity
densification

ABSTRACT

This paper discusses the role of physical structure alterations on three binder types: plain portland cement, fly ash-based binder and calcined clay-limestone binder. The kinetics of physical structure development and the relevance in transport properties were distinguished using an interlinked parameter in concrete and paste. A systematic experimental investigation was carried out on a range of critical parameters such as strength development, resistivity development, transport characteristics and the time-dependent change in transport parameter. The role of microstructure in terms of the chemical composition of C-A-S-H and its physical states in the different systems is identified as the critical factor governing the development of microstructure. Chloride resistance was assessed by chloride migration experiments for a period of 4 years. The durability behaviours of the concrete with various binder were generalised using pore network parameters such as formation factor and tortuosity. A sensitivity analysis was used to dissect the contribution of the pore solution dilution and pore connectivity to the change in the pore network parameter.

Based on the rise in macroscopic physical characteristics (i.e., formation factor here), a two-fold structure development mechanism to conceptualise microstructural evolution in cement composites is presented. Initially, capillary pore space reduces to a critical size range (i.e., 10–30 nm), which is followed by the densification of the physical state of the microstructure. At the point of densification, the pores become largely disconnected which leads to a dramatic increase in the formation factor. The binding matrix in calcined clay concretes reaches the critical pore size at an early age which leads to early densification of capillary pore space region in comparison to fly ash concretes.

1. Introduction and background

The recent surge in research studies on concrete additives is focused around the need for sustainable solutions and energy-efficient binders [1–3]. There is a considerable level of advocacy to evolve alternative clinkers and binder substitutes to meet global demand by sustainable adoption of technology [4–6]. UNEP report has laid out that cement substitution is one of the critical measures to decarbonise cement industry [7]. In this regard, several composite cementitious materials with co-substitution of multiple extenders to portland clinker are increasingly being explored in the cement industry. The use of calcined clay and limestone has emerged as one of the prominent solutions because of the ability to meet the volume of demands in cement production [8,9]. A mixture of portland clinker, limestone and calcined clay is known as limestone calcined clay cement (referred to as LC3 hereafter) [10]. The newly developed LC3 formulations take advantage of the use of lower-grade calcined kaolinitic clays [11] and also a range of different carbonate sources including limestone, dolomites and marble dust [12,13]. This combination of calcined clay-limestone produces a synergistic chemical interaction. The binder formulations with calcined clay-limestone produce nearly 30% reduction in CO_2 emissions in comparison to plain portland cement [14]. The early age mechanical properties and chloride resistance are significantly improved for concretes made with LC3 binder [15,16]. However, a clear understanding of the microstructure-dependant factors that lead to these superior performance characteristics in concrete is not available. More often, the reduction in pore sizes due to rapid development of microstructure is directly put forward to explain the variation in durability performance [17,18]. The role of these composite binders on the evolution of durability parameters can be altered owing to the difference in proportions of hydrate phases in comparison to traditional cement systems. The differences can arise due to variation in the nature of physical structure, kinetics of microstructure development, chemistry of the solid hydrates and pore solution. It is also important to distinguish between the

---

* Corresponding author.
E-mail address: manus@iitm.ac.in (M. Santhanam).

https://doi.org/10.1016/j.cemconres.2019.105959
Received 31 October 2019; Accepted 17 December 2019

contributions arising from these individual components. Therefore, the governing factors controlling durability performance need to be carefully evaluated to theorise the mechanisms by which the different components present in microstructure contribute to performance.

In general, the alterations in capillary pore space as a consequence of the early pore refinement lead to significant benefits in transport characteristics of calcined clay binders [17,18]. Further, ionic transport is governed by the combined effect of all components present in the microstructure. For instance, considering concrete as a two-phase medium with bulk solid and pore solution, the ionic transport can be affected by pore structure and ionic strength of pore solution present in the capillary porosity. The hydration products along the capillaries are mostly porous, and this makes the pore network in a hydrated cement matrix always connected due to loosely packed hydration products in the outer region. The finer size range of these hydrates leads to highly tortuous nature of the connected pores in this region which is dominated by C-A-S-H, ettringite and AFm phases. However, the connectivity keeps reducing over time at a macroscopic scale, due to progressive deposition of hydration products in the capillary region. This reduction occurs more dominantly in cementitious systems with supplementary cementing materials (SCMs), because of the continuous formation of (low-packing density, LD) C-A-S-H.

Additionally, a binder made of aluminosilicate-limestone combination contains a higher amount of the carbonate-based AFm phases (mono-aluminium ferrite phases), which can also impact the physical structure. Besides, the extent of impact can also vary based on reactivity controlled by dissolution rate of SCMs, hydration period and composition of C-A-S-H produced in the porous capillary region. The spatial distribution of the hydrates in the capillary region leads to complexity in structure development. In ternary binders with limestone, it is common to observe additional amounts of sulphoaluminate (i.e., AFt) and carboaluminate phases [19]. These phases have lower density states [20] than C-A-S-H forms, which provides improved solids coverage in the capillary pore space region. Indirectly, the hydrate formation can lead to many-fold changes in the concrete microstructure at both early and later ages.

The initial free space available in the capillaries is governed by the overall packing density of the dry ingredients and water-binder ratio. Fine limestone provides sites for nucleation and improves early age reaction rate [21]. However, characterising the role of the large volume of substitute materials on later age properties such as capillary porosity and its evolution is a challenge. These characteristics can be studied by characterising the pore network parameters. The use of pore network characteristics to explain the transport parameters can facilitate to generalise the role of physical structure on durability performance in binders with varied chemistry. Recent studies by Sui et al. [22] investigated the range of different factors affecting chloride transport such as pore size, chloride binding, pore solution, and emphasised on the lack of generic framework to collectively account for the influencing factors i.e., pore sizes and pore solution composition.. Such a phenomenon needs to be elucidated based on a systematic investigation of related microstructure characteristics to explain associated concrete durability parameters. In addition, several studies on evaluation of binder types rely on prospective durability performance-based direct comparison of pore sizes [23–25]. The viability of using such simple pore volume and pore size comparisons to explain performance characteristics of different binder types as reported in previous studies needs to critically examined and appraised. According to the Nernst-Einstein equation [26], the diffusivity of the ions is directly proportional to the conductivity of the electrolyte and inversely to the valency of the ion. This indicates that the ionic transport in concrete is also strongly influenced by the ionic strength of the pore solution and the necessity of considering the pore solution composition for detailed insights into the transport characteristics in saturated conditions.

All components present in the hydrated cement matrix contribute to the development of microstructure, and the control the transport parameters. Hence, it is vital to assess and delineate the role of the different components in varied transport mechanisms. The hydrated phase assemblages and pore solution governs the chemical equilibrium present in the cementitious systems. Any increase in the amount of hydrates directly contributes to reduction of porosity of the matrix. These physical characteristics are continuously evolving due to the process of cement hydration. In the case of SCM additions, two major factors affects the composition of pore solution: i) dilution of alkalis, and ii) alkalis binding to C-A-S-H [27]. Both factors effectively reduce the ionic strength of the pore solution. A mere addition of filler such as quartz/limestone can lead to just dilution of concentrations in pore solution, which could have implications on ionic transport. This aspect is not well explored in the existing literature.

The kinetics of structure development at later ages has significant implications for durability characterisation. Especially in blended cements, there is a dominant development of physical structure at later ages due to pozzolanic C-A-S-H formed in the capillary region. As the movement of external ions occurs in the region, the mechanism of hydrate formation governing the kinetics of structure development is critical to understand the variation in durability performance in different binder composites.

2. Research significance and goals

The present study explores the pore network parameters in different binder systems, in order to conceive the association between structure development and transport characteristics using microstructure-based factors. The combined influence of pore structure, binder chemistry and pore solution are considered to explain the chloride transport characteristics and its evolution over time. A generalised framework is established to rationalise the performance driving factors over a range of binder compositions. A clear distinction of the contribution from different components associated with microstructure is attempted. Such a distinction can help to probe the underlying mechanism of structure development and help conceptualise the contribution of microstructure to durability performance. Also, the paper presents an understanding of the multiplicity of interactions from different constituents of varied reactivity and its contribution to the kinetics of physical structure development. The role of formation factor as key microstructure-based parameter to study range of concrete mixture and binder types is also critically appraised. Also, the theoretical basis for difference in ageing factor based on the characteristics of SCM's reactivity is emphasised.

A systematic approach was adopted to study paste and concrete with three binders which include OPC, fly ash binder (at 30% fly ash content) and LC3 binder, with the investigations focused on:

a) The development of physical structure by electrical conductivity and strength in cement paste made of three binder combinations at varying water-binder ratios
b) The evolution of performance parameters such as resistivity, formation factor and long-term resistance to ingress of chloride salts in macroscopic concrete systems to determine time dependency of the transport parameter.
c) A detailed characterisation of the microstructure to establish the relationship between the microstructure parameters and performance indicators and to highlight the governing mechanisms of structure development.

3. Materials and methods

3.1. Binder composition and mixture formulation

The binders used in the study include a control binder made of ordinary portland cement (OPC), fly ash binder made of 70% OPC + 30% Class F fly ash (named as FA30), and limestone calcined clay cement made with a combination of 31% calcined clay +15%

Table 1
Chemical composition of materials used in the study.

Oxides		CaO	SiO_2	Al_2O_3	Fe_2O_3	MgO	Mn_2O_3	Na_2O	K_2O	TiO_2	SO_3	LOI
OPC		64.59	19.01	4.17	3.89	0.88	–	0.16	0.59	0.23	1.7	1.4
Class F fly ash		1.28	59.32	29.95	4.32	0.61	–	0.16	1.44	–	0.16	–
LC3	Clinker	63.81	21.12	5.24	3.41	3.06	0.06	0.32	0.19	0.1	0.63	0.98
	Calcined clay	0.09	58.43	24.95	5.08	0.19	–	0.05	0.21	1.41	–	9.58
	Limestone	48.54	10.07	1.74	1.62	0.467	0.04	–	0.13	0.21	0.01	37.09

limestone replacing OPC. The chemical composition of constituents is given in Table 1. The mean particle size of OPC, fly ash and LC3 were 18.50, 15.50, 13.00 μm respectively, as determined by laser diffraction analysis.

Cement paste was prepared with water-binder ratios of 0.3, 0.4 and 0.5. The paste was cast in a prismatic acrylic mould (40 × 40 × 100 mm) for electrical conductivity measurements and filled in a polyethylene container for microstructural studies. Polycarboxylic ether-based superplasticizer was added to the paste with 0.3 water-binder ratio to improve the fluidity of paste for fabrication.

Three concretes mixes were prepared with each binder. The concrete mixture proportioning is elaborated elsewhere [15]. Three binder contents and range of water-binder ratios between 0.4 and 0.6 were adopted to prepare concretes for compressive strength evaluation using 150 mm cube specimens. The fine aggregate used for the concrete was graded river sand with 4.75 mm nominal maximum aggregate size, and a mixture of 10 mm and 20 mm crushed granite was used as coarse aggregate. A polycarboxylic ether based superplasticiser was used to achieve the target slump of 80–120 mm. The concretes were mixed in a pan mixer at 25 rpm and concretes were fabricated in a temperature of 27 ± 3 °C. The fresh properties such as initial slump and fresh unit weight were measured. The specimens were cast and placed in a laboratory condition for a period of 24 h, after which the demoulded concrete specimens were moved to a moist room (>90% RH) until the specified age of testing.

The details of the nine mixes chosen for further investigation are given in Table 2. The two strength grades include M30 and M50 (indicating a 28-day characteristic compressive strength of 30 and 50 MPa respectively), which are representative of a normal strength concrete and moderately high strength concrete used in major applications. Apart from the two equivalent strength grade mixes, an additional concrete mix with the same binder content and water-binder ratio was also chosen as a benchmark to assess the performance between different binder systems.

3.2. Assessment of macro-scale properties on paste and concrete

3.2.1. Development of strength and conductivity in cement paste

Cement paste was cast into 50 mm cubes for compressive strength measurements. The specimens were wrapped and sealed to avoid any loss of water after fabrication. After 1 day, the specimens were demoulded and placed in a moist room until the age of testing. The hardened density of the paste specimens was checked before compressive strength measurements, and the variations were found to be limited at all ages. Cement paste cubes were tested at rate of 900 N/s. The average compressive strength of three specimens is reported for each data point.

For the electrical conductivity measurement, the paste was filled in acrylic moulds of 100 mm × 40 mm × 40 mm immediately after mixing. This mould was fitted with stainless steel plates on both sides to act as electrodes for impedance measurement. The specimens for impedance measurement were kept saturated in a wet room (>90% RH) and covered with a damp cloth to prevent drying of specimens. Impedance response was captured using a Solartron 1260 instrument between a frequency range of 0.1 Hz–1 MHz with an AC voltage of 250 mV. The intersection point of the bulk and electrode arcs from the Nyquist plot was considered as the resistance of the bulk cementitious systems to calculate electrical conductivity from paste systems, as reported in previous studies [17,28].

3.2.2. Transport parameters in concrete

A Wenner 4-probe resistivity meter (Resipod resistivity meter) was used to measure resistivity on saturated cylindrical specimens of 100 mm diameter and 200 mm height [29,30]. Each data point is an average of 27 measurements taken at three different locations on the cylindrical surface of the specimens. A scatter plot showing a cluster of data from one measurement at a particular age is given in Fig. 1. Typical spread in surface resistivity measurements. All measurements were taken on saturated specimens in a moist room at a temperature of 23 ± 3 °C.

Additionally, the resistance to chloride ingress was evaluated using a migration experiment as per NT Build 492 1999 [31]. The resistance measured by the initial current was used to estimate electrical conductivity by ASTM C1760 [32]. Water accessible porosity was determined by vacuum saturation on 30 mm thick specimens. The mass of the dried and saturated specimens was measured to an accuracy of 0.01 g. The measurements were made on four concrete slices of 30 mm thickness prepared from concrete cores (70 mm diameter) taken from a 150 mm cube. The specimens were conditioned in a 50 °C oven for 7 days before subjecting to standard vacuum saturation process [33].

A part of the data, notably resistivity, porosity and chloride migration coefficient at 28 days and 90 days is published in [15] and

Table 2
Mixture design of concretes studied.

Grade			M30			M50			Common Mix		
Binder type			OPC	FA30	LC3	OPC	FA30	LC3	OPC	FA30	LC3
w/b			0.5	0.45	0.5	0.4	0.35	0.4	0.45	0.45	0.45
Binder content		kg/m^3	310	310	310	360	380	340	360	360	360
Water			155	139.5	155	144	133	136	162	162	162
Fine aggregate			695	723	708	703	699	704	721	721	687
Coarse aggregate	10 mm		496	491	491	477	475	488	463	463	476
	20 mm		744	737	736	716	713	732	694	694	715
Unit weight			2371	2414	2487	2385	2406	2463	2399	2385	2414
SP	(solid% by wt. of binder)		0.02	0.65	1.00	0.65	0.60	0.85	0.10	0.23	0.36
Slump		(mm)	100	100	80	90	120	120	90	90	120

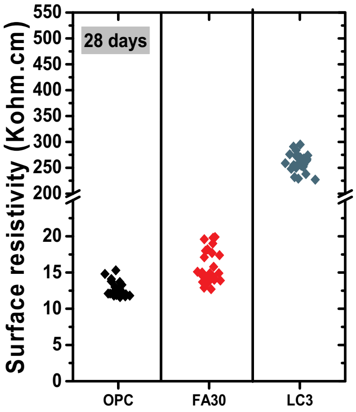

Fig. 1. Typical spread in surface resistivity measurements.

reused for analysis along with additional data presented in this paper. The discussions of the results in this paper are enhanced by the determination of the formation factor and tortuosity of the pore network in the system. Formation factor can be a representative durability indicator and this is acknowledged in AASHTO PP-84 [34]. The formation factor (also known as formation resistivity factor [35]) is the ratio of conductivity of pore solution to the conductivity of bulk concrete. The total porosity, interconnectivity of the pore space and ionic concentration in pore solution influences the conductivity of bulk concrete. Hence, the formation factor represents the normalised conductivity of the systems which respect to the pore solution of the system. Formation factor is closely related to the characteristic capillary porosity in the hydrated cement matrix [17]. The bulk conductivity of cement systems is the response of the ion filled pores i.e., pore solution, total porosity and connectivity of ion filled pores. Further, the relationship between effective bulk conductivity (σ_{eff}), porosity (ϕ), and pore solution conductivity (σ_o), given in Eq. (1), is used to obtain pore connectivity factor (β) [36]. The pore connectivity factor is used to estimate electrical tortuosity by the inverse square root relationship shown in Eq. (2), as suggested in [37].

$$\sigma_{eff} = \phi\beta\sigma_o \tag{1}$$

$$\tau = \frac{1}{\sqrt{\beta}} = [F.\ \phi]^{0.5} \tag{2}$$

Here, τ is the electrical tortuosity, F is the formation factor (unitless), and ϕ is the water-filled porosity of concrete (volume fraction). The tortuosity relationship considers the connectivity in the microstructure is governed by single dominant pore size as described in [37] (see Eq. (2)). In simple terms, tortuosity is a geometric parameter which indicates the state of the complex pore network in the microstructure. However, in this case, the tortuosity obtained from electrical measurement is indicative of the traverse path of charged ionic species (i.e., diffusive pathway of an ion) in a concrete system.

3.3. *Microstructural characterisation of cement paste*

Several characterisation techniques were used to probe the differences in the microstructure of pastes with different binder systems, which includes the study of hydration products by XRD, pore structure using mercury intrusion porosimetry, pore solution composition using inductivity coupled plasma emission spectroscopy (ICP-ES) and characterisation of CSH using SEM and nanoindentation technique. The hydration was stopped by storing the paste specimens in isopropanol for 4 days [38]. After 4 days immersion, the samples were dried for a minimum period of 3 days in a vacuum desiccator.

For observing microstructural features and estimating the chemical composition of C-A-S-H forming at different ages, the scanning electron microscope was used in the Back-Scattered Electron (BSE) mode along with energy-dispersive X-ray spectroscopy (EDX). Thin slices from the paste specimens (after hydration stoppage) were epoxy impregnated (under vacuum), polished with diamond spray (up to 1 µm) and coated with carbon. Statistical evaluation of EDX measurements was carried to capture a representative value of the chemical composition of microstructure. A typical EDX measurement on a BSE image and scatter in data acquired is given in Fig. 2.

Pascal 140–440® Mercury Intrusion Porosimetry (MIP) instrument from Thermo Scientific was used to measure pore size in the range of 100 µm to 3 nm. The methodology of sample preparation and testing protocol is elaborated in [17]. Several small fragments of paste (<4 mm thickness) and mortar chunks from concrete were used for porosimetry measurements. Also, paste specimens after hydration stoppage were tested using PANalytical diffractometer. The diffractograms obtained from XRD were analysed through PANalytical Xpert High Score Plus Software V.4 for phase identification and quantitative estimation by external standard method. A goodness of fit around 2 was ensured to confirm the reliability of the analysis.

A Hysitron Triboindenter nanoindentation instrument was used to probe the micromechanical characteristics. The stiffness parameter, which indicates the packing density of the C-A-S-H hydrates, was studied by applying a small load of 2000 µN using Berkovich indenter. The load-displacement response was made on a series of points in the form of 15 × 15 matrix with a spacing of 10 µm to obtain a statistically significant number of data points. The deconvolution of the probability

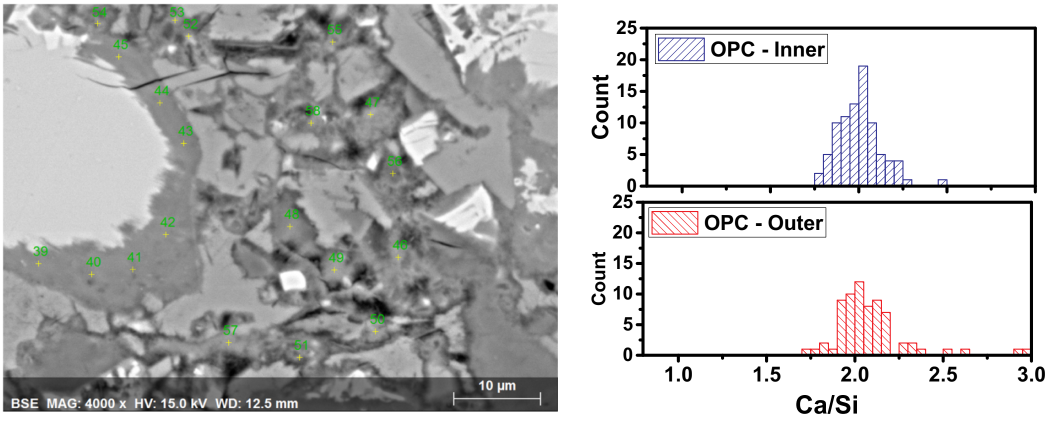

a) b)

Fig. 2. Typical measurement of EDX on a cement paste and representative scatter in the EDX data for about 100 measurements.

densities from indentation modulus evaluated over a matrix of 225 data points showed three significant regions of hydrate moduli (10–70 GPa). Care was taken to eliminate the interference due to porosity based on the load-displacement profile.

The alkali content was measured on the pore solution extracted using a mechanical press, as suggested in [39]. The cement paste was prepared with a water-binder ratio of 0.5 and allowed to hydrate in a sealed condition (enclosed with paraffin film) for 28 days in a cylindrical polyethene container. The extracted solution was analysed using inductively coupled plasma emission spectroscopy (ICP) for the calcium, sodium and potassium ions. The summation of concentration of ionic species multiplied by equivalent conductivity contributed by the corresponding ionic species was used to compute the electrolyte conductivity of the pore solution as suggested in Snyder et al. [40]. The equivalent conductivity was estimated using Eq. (3). The effective conductivity of pore solution ($\sigma_{pore\ soution}$, S/m) was obtained as a summation of the product of valence of the ion (z_i), concentration (c_i, mol), and conductivity of an ionic species in infinite dilution (σ_i, S/m/mol), which is a function of conductivity coefficient and ionic strength (I_M,mol/L), as given in Eq. (4) [40].

$$\sigma_i = \frac{\sigma_i^o}{1 + G_i.\ I_M^{0.5}} \tag{3}$$

$$\sigma_{pore\ soution} = \sum_i z_i.\ c_i \sigma_i \tag{4}$$

4. Results and discussion

4.1. Strength and resistivity development

4.1.1. Compressive strength development in cement paste

The paste compressive strength development indicates the macroscopic property of the bulk matrix and its contribution to the mechanical properties of concrete. The relative alteration in compressive strength development due to the water-binder ratio was studied to assess the potential for strength gain at varied capillary porosity, as outlaid in the gel space ratio concept [41]. The amount of initial free water can directly control interparticle spacing which develops as the capillary porosity region and thereby influences the strength development. High volume substitution in the calcined clay-limestone binder can alter the development of properties as there is more demand on the pozzolanic reaction to produce solid hydrates in capillary pore space to mask the dilution of clinker compounds.

Fig. 3 presents the strength development of pastes with different binders at a range of water-binder ratios (i.e., 0.30, 0.40 and 0.50). The strength development was found to be consistent for all binders, with an increase in compressive strength for reduction in w/b ratio from 0.50 to 0.30. Also, reduction in water-binder ratio below 0.40 produced a substantial rise in mechanical properties across curing ages. The OPC paste showed minimal changes in compressive strength post 28 days at higher water-binder ratios. The initial strength of FA30 paste was marginally lower than OPC up to 7 days and was found to be less altered by the reduction in w/b ratio. The slow reactivity and dilution effect of fly ash limits the benefit of reducing w/b from 0.50 to 0.30 at early ages in FA30 paste. The difference in strength due to w/b was prominently visible only by 7 days. Between 7 days and 28 days, the FA30 paste showed a substantial rise in strength due to the fly ash reaction making prominent contribution during this period (Fig. 3b). At this stage, the difference in strength due to w/b becomes substantial, nearly doubling from 40 MPa (FA30 with w/b of 0.50) to 80 MPa (FA30 with w/b of 0.30). Further, compressive strength of FA30 paste was found to increase continuously up to 90 days due to sustained reaction.

In LC3 binder, a significant rise in early age compressive strength occurred with a reduction in w/b ratio from 0.40 to 0.30. The acceleration in hydration characteristics due to limestone and calcined clay was able to take advantage of lower free capillary space and produce a significant difference in mechanical properties by 1 day of hydration. Unlike FA30 systems, LC3 paste showed a significant leap in compressive strength between 3 and 7 days at all w/b ratios (see Fig. 3c). The interaction of calcined clay reacting in the hydrating matrix leads to earlier convergence of capillary porosity (reported in [17,42]) due to better space-filling characteristics (i.e., more volume of solid hydrates and reduced total porosity). This alteration in hydration characteristics led to a systematic increase in strength at all w/b between 3 days and 7 days, and the strength continued to rise until 56 days of curing. The benefit in compressive strength with a reduction in water-binder ratio was noticed from early ages (i.e., 1 day and 3 days) denoting the positive response of improved hydration characteristics of LC3 binder. However, the FA30 paste started to show a marked distinction for cement paste at 0.40 w/b and 0.50 w/b only by 7 days and 28 days due to lower reactivity of fly ashes. This difference indicates the reduced potential of slowly reactive SCMs such as fly ashes to positively influence strength development at early ages despite a reduction in w/b ratio. Fig. 3d presents the strength gain for the three binders at 0.40 w/b, which shows the ability of LC3 to produce similar strength development rate to OPC. FA30 systems showed steady rise post 7 days to catch up with the other binders by 56 days.

Additionally, the strength development at 0.30 w/b suggested that OPC reaches a higher ultimate strength. Paste with OPC showed a strength of 90 MPa at 90 days of curing, while FA30 and LC3 paste showed 83.9 and 72.5 MPa, respectively. This could be attributed to the contribution of the unreacted clinker particles present in OPC systems that have higher stiffness and hence, higher impact on compressive strength of plain portland cement or binder systems with higher clinker content [43]. Also, the characteristics of pozzolanic gels formed in blended binders can affect the contribution to strength. The low-stiffness state of low Ca/Si pozzolanic C-S-H can lead to a differential contribution to physical structure (i.e., porosity and pore connectivity) and mechanical response (i.e., strength) with greater impact on the former than the latter.

4.1.2. Conductivity development in cement paste

The amalgamated electrical response from evolving cementitious systems contains information of bulk characteristics such as the total volume of pores, connectivity state of pore volume, ionic strength of the pore fluid and the capacitance of the solid phase. There is a continuous variation in the relative proportions of these components which reflect the development of physical structure in different binder systems. For particular cementitious systems, the change in conductivity response is predominantly affected by the evolution of the pore volume and interconnected pores present in the hydrated cement matrix [44]. Thus, electrical response, i.e., conductivity or resistivity measurements from cementitious systems is an ideal technique to track the kinetics of pore structure evolution in hydrating cementitious matrix by a continuous non-invasive assessment. However, there can be some false positive signals due to reduction in pore solution concentration. This interference can be decoupled by considering pore solution composition in a generalised form for comparison across different binder chemistry, in order to enable assessment of the pore network characteristics alone. In composite cement with SCMs, the major distinctions in the electrical conductivity can be observed mainly due to the interactions between components in the binder systems (such as SCM reaction) and water-binder ratio of the hydrating matrix.

The evolution of electrical conductivity of the binder systems at various w/b is given in Fig. 4. In OPC, the change in conductivity beyond 14 days is trivial. Note that w/b has a permanent effect on the evolution of the conductivity and maintains a considerable difference across all ages. This impact can be noticed from the band of conductivity values in OPC, which maintains an order $0.30 < 0.40 < 0.50$ w/b. Also, the difference was sustained at later ages up to 400 days. The results also show improved kinetics of physical

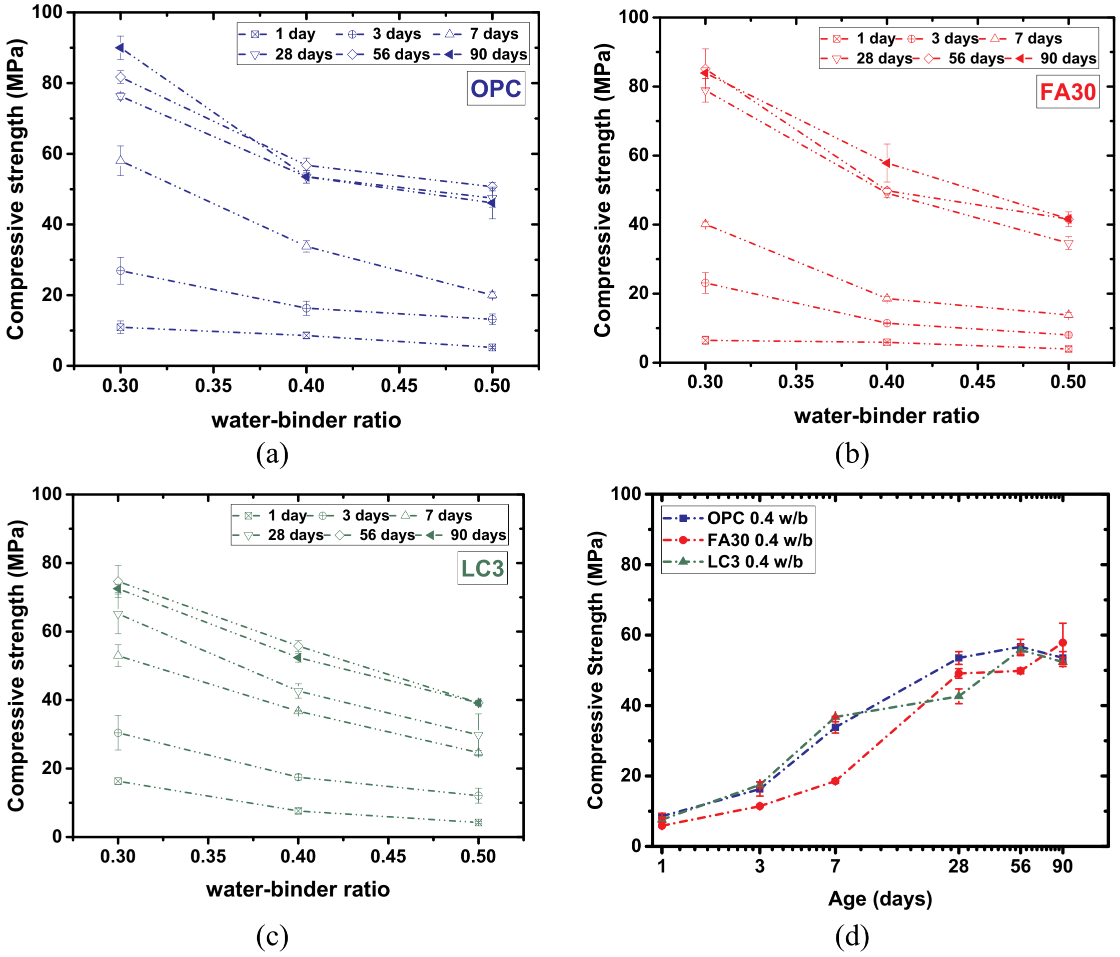

(a) (b)

(c) (d)

Fig. 3. Compressive strength development in cement paste. (a) OPC, (b) FA30, (c) LC3 binder with varying water-binder ratios and (d) strength development rate at 0.4 w/b.

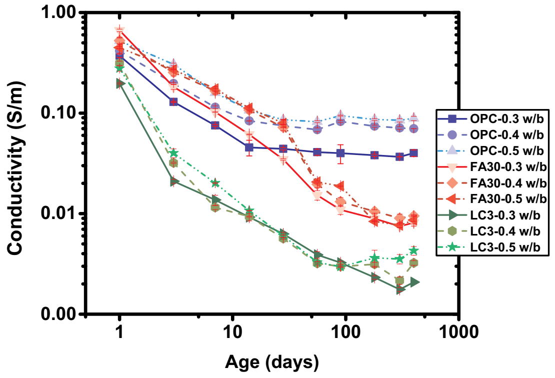

Fig. 4. Evolution of electrical conductivity in the pastes with OPC (blue), FA30 (red), and LC3 (green) at the different water-binder ratios. (For interpretation of the references to colour in this figure legend, the reader is referred to the web version of this article.)

structure development due to reduction in w/b for OPC systems. However, lower w/b ratio does not necessarily invoke progressive reduction in conductivity at later ages in plain portland cement.

The conductivity value in FA30 mixes was higher than OPC in the early curing period (i.e., until 14–28 days) due to the delayed interaction of fly ash (see Fig. 4). The dilution in hydrates due to fly ash addition results in more porous cementing matrix and increases the conductivity value in comparison to OPC systems during this regime [17,45]. In distinction to the OPC system, a steady drop in conductivity can be noticed beyond 14 days for FA30 paste across water-binder ratios, which is a signature of fly ash reaction in the microstructure. The continual change in the physical structure of hydrating systems at different stages of hydration affects the conductivity response of fly ash pastes: i) the dilution in hydrates results in higher amount of connected pores at early ages and ii) pozzolanic reaction reduces porosity and pore connectivity dominantly at later ages. The results of FA30 across water-binder ratios show that reducing w/b accelerates the kinetics of conductivity change and produces marginally improved reduction in conductivity at an early age. However, the kinetics of three binders are quite distinct which indicates the crucial role of reactivity of the ingredient present in the binder. For example, FA30 with higher water-binder ratio (i.e., 0.40 and 0.50) shows a substantial drop in the conductivity by 28 days and gives similar reduction beyond 28 days at different w/b. A distinct reduction in the FA30 pastes at higher w/b can be due to the availability of more porosity for pozzolanic gel formation to occur in the microstructure, denoting the space-bound kinetics of the binder reactions (in blended systems). The impact of pozzolanic reaction of fly ash continuously diminishes once the microstructure is densified as pores can become limited (in size and quantity) for further hydration to occur. Also, it can be seen that the change in conductivity again becomes trivial by 180 days for FA30 at all w/b ratios. Despite reduction in w/b, the slow reactivity of the fly ashes delays the onset of the drop in conductivity and thus, the reduction of the pore structure. The water-binder ratio is one of the major factors controlling the initial pore space provided to the anhydrous materials to react and thereby, dominates the time-dependent space-filling mechanism to limit the reaction kinetics to some extent [24]. Surprisingly, the benefit in conductivity development due to reduction in w/b within a particular binder type was insignificant in comparison to the benefit achieved by actually changing the binder composition. Thus, it becomes essential to understand the influence of these variations on the long-term durability properties.

In the case of LC3 binder, the conductivity values show a significant reduction at early ages, i.e., between 1 day and 7 days. The high reactivity of the calcined clay ensures that the variation due to the water-cement ratio is also markedly converged by 14 days. This convergence can be attributed to the space-governed kinetics of structure development, similar to FA30 systems at later ages. The conductivity drop in LC3 binder reaches a state of almost no change by nearly 100 days, possibly due to the limitation in the pore volume. The pozzolanic C-A-S-H produced in the calcined clay systems has an exceptional ability to cause convergence of solid hydrates due to space-filling ability of the LD-C-A-S-H [46,47]. Thus, the characteristics of the C-A-S-H, which leads to such minimal difference in the conductivity evolution across w/b ratios, is critical to understand. In general, it is clear that the variation in conductivity due to w/b ratio was narrowed down due to pozzolanic reaction of fly ash and calcined clay, unlike OPC which does not sustain reactions at later ages. Additionally, the fact that the bridging occurred earlier in the paste with calcined clay mixes than fly ash system carries a direct implication for the improved physical structure in the concretes made with LC3 binder for a range of mixture proportions, i.e., binder and water contents. The results also provide fundamental insight on the role of binder characteristics on the performance of concretes made with these binder systems. One such implication from the trends is that the traditional plain portland cement could require a significant reduction of w/b ratio to ensure compliance with the required durability parameter. In the case of the composite cement with SCMs, sufficient curing can ensure the durability compliance without significant reduction of the water-binder ratio in the concrete mixtures with SCMs.

The credibility of the conductivity measurement to represent the physical state of the microstructure is explored by investigating the relationship between the strength and conductivity of the three binder systems. Fig. 5 presents the changes in compressive strength as a function of conductivity for all three binders. OPC systems show a systematic increase in strength with a reduction in conductivity, confirming the influence of lowered capillary porosity. In FA30 and LC3, the early age data fit quite well along with the trends of OPC. However, the data start showing drift towards lower conductivity values for response obtained at later ages. The drift occurs earlier in the case of LC3 compared to FA30 systems. With hydration time, the conductivity showed a dramatic reduction for FA30 and LC3 due to alteration in physical structure from fly ash and calcined clay reactions, which reduces pore connectivity and not necessarily total pore volume as hydrates produced in capillaries stay mostly connected. Thus, this reduction in conductivity does not directly reflect as a major rise in compressive strength. Additionally, the deviation from the OPC curve can mark the stage of pozzolanic C-A-S-H impacting the microstructure significantly. The trends confirm the substantial contribution of pozzolanic C-A-S-H to physical structure, i.e., pore connectivity, which occurs significantly earlier in the LC3 paste as compared to the fly ash paste.

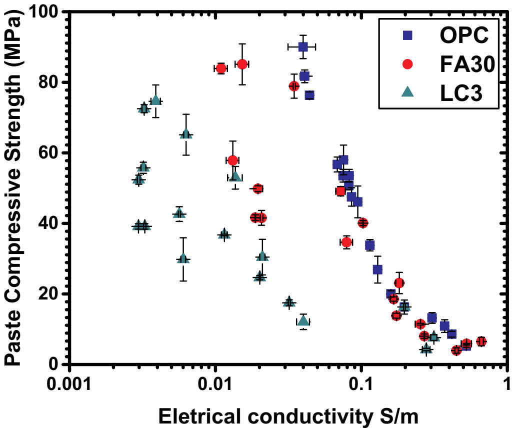

Fig. 5. Incongruent relationship between paste compressive strength and electrical conductivity for each binder type.

4.1.3. *Compressive strength development in concrete*

Compressive strength development was assessed for the three categories of concretes at 3, 28 and 90 days. Fig. 6(a), (b) and (c) presents the results for M30, M50 and C-mix, respectively. In all cases, the early strengths of LC3 concrete (i.e., 3 days) were found to be significantly higher than FA30 concrete in all category of concretes. At 3 days, FA30 concretes had lower strength despite reduction in w/b to produce similar 28 days strength in the equivalent strength category. This reduction reaffirms the sensitivity of LC3 binder to respond to changes in w/b at early ages, as observed previously in the strength development of FA30 and LC3 paste. In C-mix concretes, the strength development was nearly similar for OPC and LC3. The strength of FA30 concrete steadily increases over time up to 90 days as shown in Fig. 6(c). The strength and electrical conductivity (as per ASTM C1760) relationship between binder types were explored in concretes and found to be similar to that identified in cement paste. The trends in Fig. 6(d) shows the distinction between binder types based on the conductivity-strength relationship, which is progressing at varied rate for OPC, FA30 and LC3 binders. A distinct difference in the electrical conductivity in the order OPC < FA30 < LC3 can be noticed. The variation in pore solution conductivity, difference in connectivity of pores, and volume filling ability of pozzolanic hydrates present in these systems lead to such differences in the behaviour between the different binder systems. The results also suggest that concretes made with different binder types can produce similar strength grades with entirely different transport indices such as electrical conductivity. A strong basis to explain the difference in the behaviours of the three binder types is identified as critical for further exploration in the present work.

4.1.4. *Resistivity development in concretes*

The role of concrete mixture proportioning on the development of concrete properties was studied to assess the role of binder type on the performance parameters of concrete systems. The results of surface resistivity and formation factor are presented in Fig. 7. Concrete surface resistivity is a useful durability parameter and is commonly used in several durability specifications [29,48]. For each binder, the band shows the average of 81 measurements done on all 9 concretes specimens (3 each in M30, M50 and C-Mix concrete which includes 27 measurements done on three circumferential surfaces) with deviation as seen in Fig. 7(a). The surface resistivity measurement was in tune with the changes in electrical measurement done on cement paste. The surface resistivity for concretes with LC3 was significantly higher at an early age and continued to rise until nearly 400 days. At 28 days, the resistivity value of fly ash was only marginally higher compared to OPC and then showed a major rise post 28 days. The value of OPC is least impacted due to hydration time in comparison to concretes with FA30 and LC3, which is similar to bulk conductivity changes in cement paste at the different water-binder ratio. This change adds substantial evidence to prove that the changes in the physical structure of cementing matrix primarily govern the development of performance parameters in concrete systems. Though the concrete mixture proportioning can be used to produce variable levels of strength and modified further to achieve desired rate of strength development, the choice of binder is crucial in attaining target durability parameters. In a study on the effect

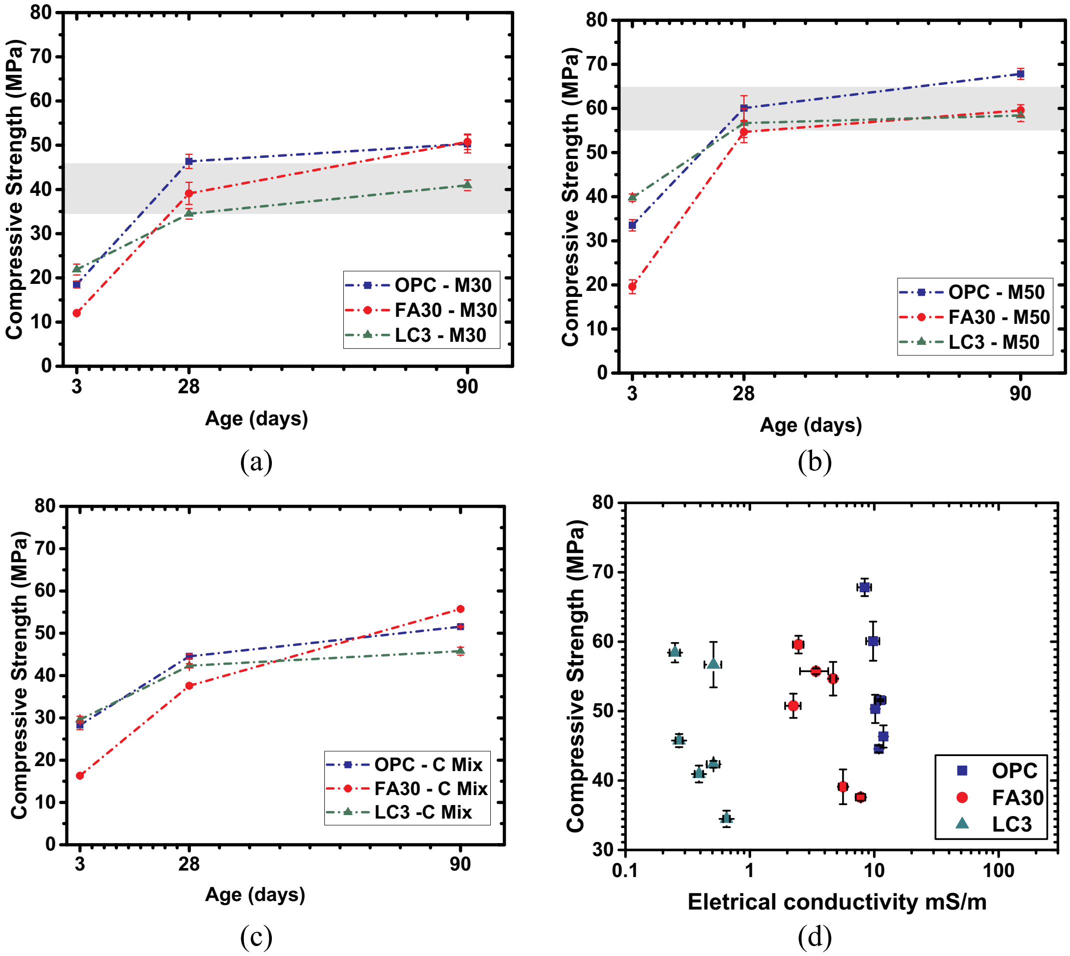

(a) (b) (c) (d)

Fig. 6. Compressive strength development in concretes (a) M30, (b) M50 and (c) C-mix and (d) Incongruent relationship between compressive strength and conductivity in concretes for different binders. Note that only 28- and 90-days results were used in (d).

of concrete mixture proportioning with LC3 binder, the resistivity was found to consistently increase between 3 and 7 days in about 27 concretes confirming the role of calcined clay [49]. For instance, as per ACI 222R classification, the data presented in Fig. 7 suggest that all concretes made with LC3 and FA30 binder have lower risk for corrosion propagation.

The intrinsic artefact in bulk electrical response due to the variation in the pore solution can be decoupled by using the formation factor approach, which considers both the bulk and solution contribution. The results from formation factor estimates are presented in Fig. 7(b). The value of formation factor presented in this study was in the range for different classes of concretes quality as per AASTHO PP-84 [50]. A distinct observation is that the resistivity value of FA30 concretes could not reach the resistivity values of LC3 concretes even up to 1 year. However, once normalised to the difference in the pore solution conductivity of individual binder systems, FA30 concretes at 1 year could

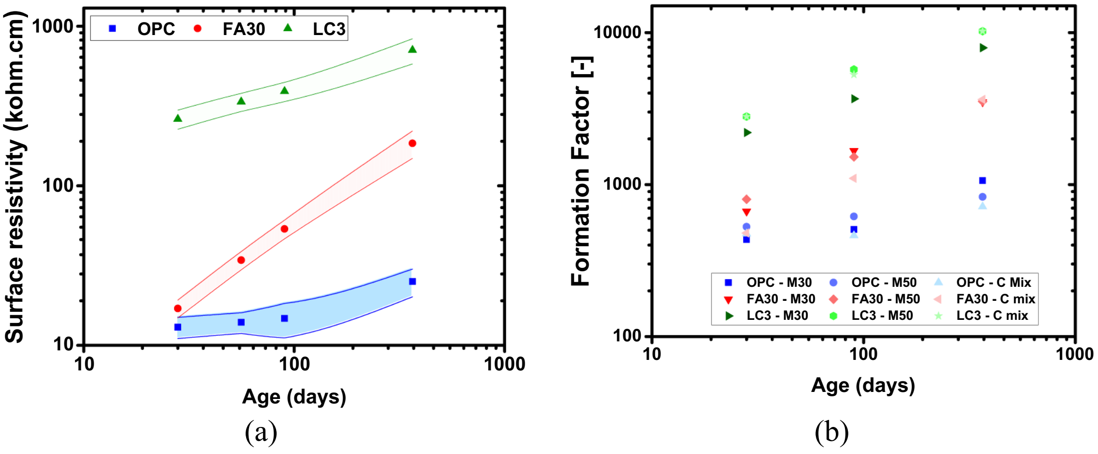

(a) (b)

Fig. 7. Development of surface resistivity and formation factor in nine concretes.

potentially reach an equivalent physical state to LC3 concrete at 90 days based on the measure of formation factor as a physical structure parameter. This distinction clearly shows the advantage of formation factor approach to account for the intrinsic discrepancy due to alteration of pore solution and to represent the physical structure state of concrete across different binder systems. To further validate the hypothesis of the use of formation factor as a microstructure-based factor, it is necessary to assess the credibility of using formation factor to represent the transport parameter across different binder systems.

4.2. Time-dependent change in the chloride transport parameter

In general, the alteration in the kinetics of microstructural development has a direct impact on the initial transport parameter and time-dependent change in transport resistance. Time-dependent change in transport resistance needs to be evaluated by examining the evolution of chloride transport parameter over a period of time. This may give insights on the ability of binder compositions to sustain the durability potential for an extended period which is specifically essential to evaluate in concrete systems with distinct phase assemblage such as LC3 in comparison to conventional binder systems. For this rationale, the chloride migration coefficient was assessed at 28 days, 90 days and 365 days for concretes cured in moist conditions until the age of testing. After that, concrete specimens were air cured post the moist curing period by placing in uncontrolled indoor conditions (Chennai conditions) until 1400 days (±50 days, between 2016 and 2019) to assess the long-term durability potential of the calcined clay-limestone binder. For air-cured specimens, the top 15 mm were removed to avoid carbonated zone affecting the chloride penetrability results. The migration coefficient was chosen for assessing chloride penetrability due to the better reliability in comparison with ASTM C1202. Also, the chloride penetrability coefficient (called the 'Non-Steady State Migration Coefficient') is estimated based on the depth of chloride penetration. The migration coefficient as a durability parameter has also found acceptability in performance-based design approaches for service life estimation in Duracrete and FIB Model Code 34 [51].

Fig. 8(a) represents the migration coefficient as a function of time and the formation factor. Concretes made with OPC had lower resistance at an early age and showed limited evolution with extended curing duration until 365 days. The migration coefficient was nearly similar for OPC concrete at 1400 days after air curing. In all binder systems, M50 concrete showed the lowest migration coefficient across ages, and the difference between concrete grades was limited only within the binder systems. The initial resistance of FA30 concrete was only marginally lower than OPC concretes. However, the migration coefficient consistently reduced from 28 days to 365 days, and further up to 1400 days. In LC3 concretes, the migration coefficient was nearly 10 times lower in comparison to OPC concretes until 1400 days (see Fig. 8). The chloride resistance of LC3 concrete continuously improved over time and nearly 50% lower migration coefficient was seen compared to FA30 concrete at 365 days, a trend which continued even at extended ages (1400 days). This difference in the behaviour of FA30 and LC3 concretes put forward the necessity to consider the combined effect of initial transport parameter and time dependency parameter to assess the actual potential of the concrete systems during the period of service in concrete structures.

Numerous factors need to be considered to explain the variation in performance parameters i.e., the difference in the ranking of initial chloride penetrability resistance and time-dependent change in the transport parameter of LC3 and FA30 concretes. The role of physio-chemical characteristics of the binder systems should be probed to reason out the root cause of such differences at later ages. The influence of pore sizes and its disconnectedness, pore solution composition, amount of aluminate-bearing hydrates and associated phase transformation can independently or synergistically contribute to resistance to chloride ingress. As chloride transport parameters were assessed in this study using electrical methods, the contribution from pore structure evolution and pore solution alone is explored further in this study.

As formation factor reflects the physical structure development in the capillary pore space, the influence of its variation on the durability performance of concrete made with different binder systems is explored. For this purpose, the results of the non-steady state chloride migration coefficient are plotted against formation factor and presented on the right side in Fig. 8. Migration coefficient and formation factor measurements up to one-year period alone were used for this analysis as concrete was continuously in a moist condition without major alteration in pore solution. The influence of the binder type is apparent with the results from the LC3 concretes showing a much lower migration coefficient and higher formation factor as compared to FA30. Both blended binders showed higher resistance to ionic ingress than OPC concretes due to the combined effect of lower porosity and pore connectivity. Also, concretes made with different mixture proportion and binder chemistry have similar chloride penetration resistance at equivalent formation factor. Thus, the relationship confirms the generic adoption of formation factor as a representative microstructure-based factor which relates to durability characteristics in a range of concretes across different binder chemistry by deconvoluting the impact of pore structure and pore solution from the bulk electrical response. The use of formation factor as a framework for explaining transport processes in concrete systems aspects has been explored in recent literature [52–54]. The combined reduction of porosity and pore connectivity, which leads to higher formation factor, can explain the influence of pore structure

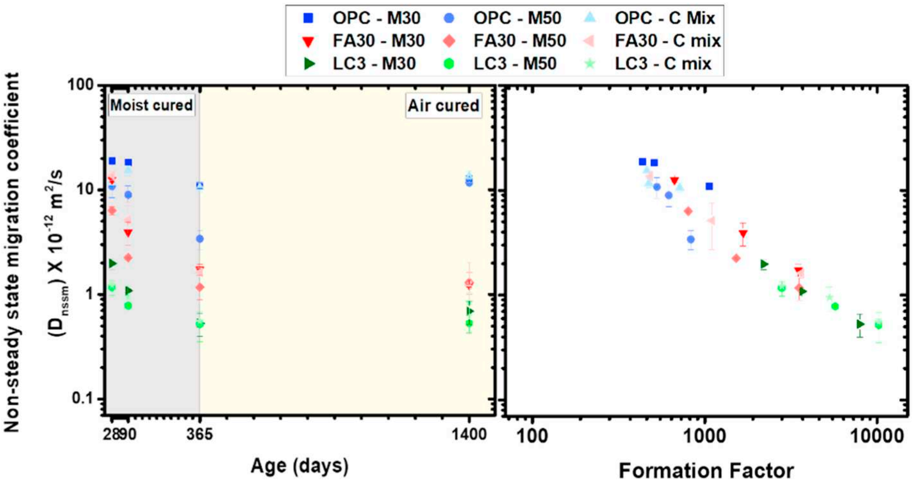

Fig. 8. Chloride transport parameter as a function of age (left) and formation factor (right).

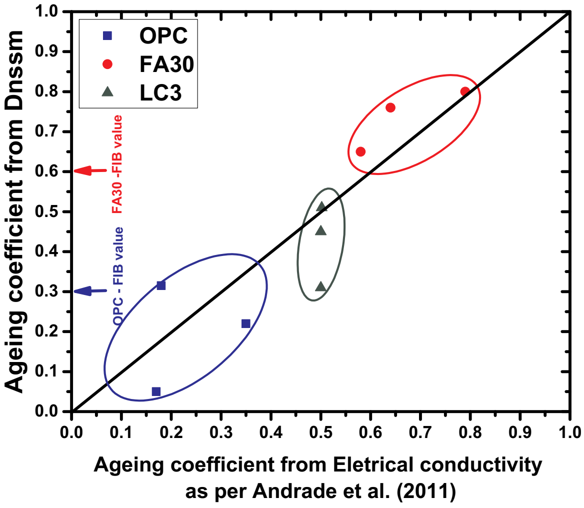

Fig. 9. Ageing coefficient of concretes from migration coefficient and electrical conductivity.

on durability parameters in composite binder systems.

The formation factor estimates of FA30 concrete were initially close to OPC systems and evolved dramatically to reach similar range as LC3 concrete. This development is due to the time-dependent evolution of the ionic resistance. The time dependency parameter, also known as ageing coefficient, can be obtained as the slope of the chloride resistance parameter and time on a log-log plot [55,56] as given in Eq. (5). The chloride migration rate measured at 28, 90 and 365 days in moist conditions is used for this purpose. Fig. 9 shows the ageing coefficient for nine concretes with OPC, FA30 and LC3 binder.

$$A(\mathbf{t}) = \left(\frac{\boldsymbol{t_0}}{\boldsymbol{t}}\right)^{a} \tag{5}$$

where A(t) is the ageing function of the transport parameter, i.e., diffusion coefficient, migration coefficient or conductivity, t_o is the time of initial measurement of transport parameter and t is the age of the concrete. The parameter 'a' is the ageing coefficient which is then obtained by regression based on Eq. (5).

The ageing coefficient accounts for the development of transport resistance and influences the service life estimates as proven in [57]. The delayed, nevertheless progressive, contribution of fly ash to pore structure and chloride resistance is captured by the higher ageing coefficient for all concretes with fly ash. The ageing coefficient was

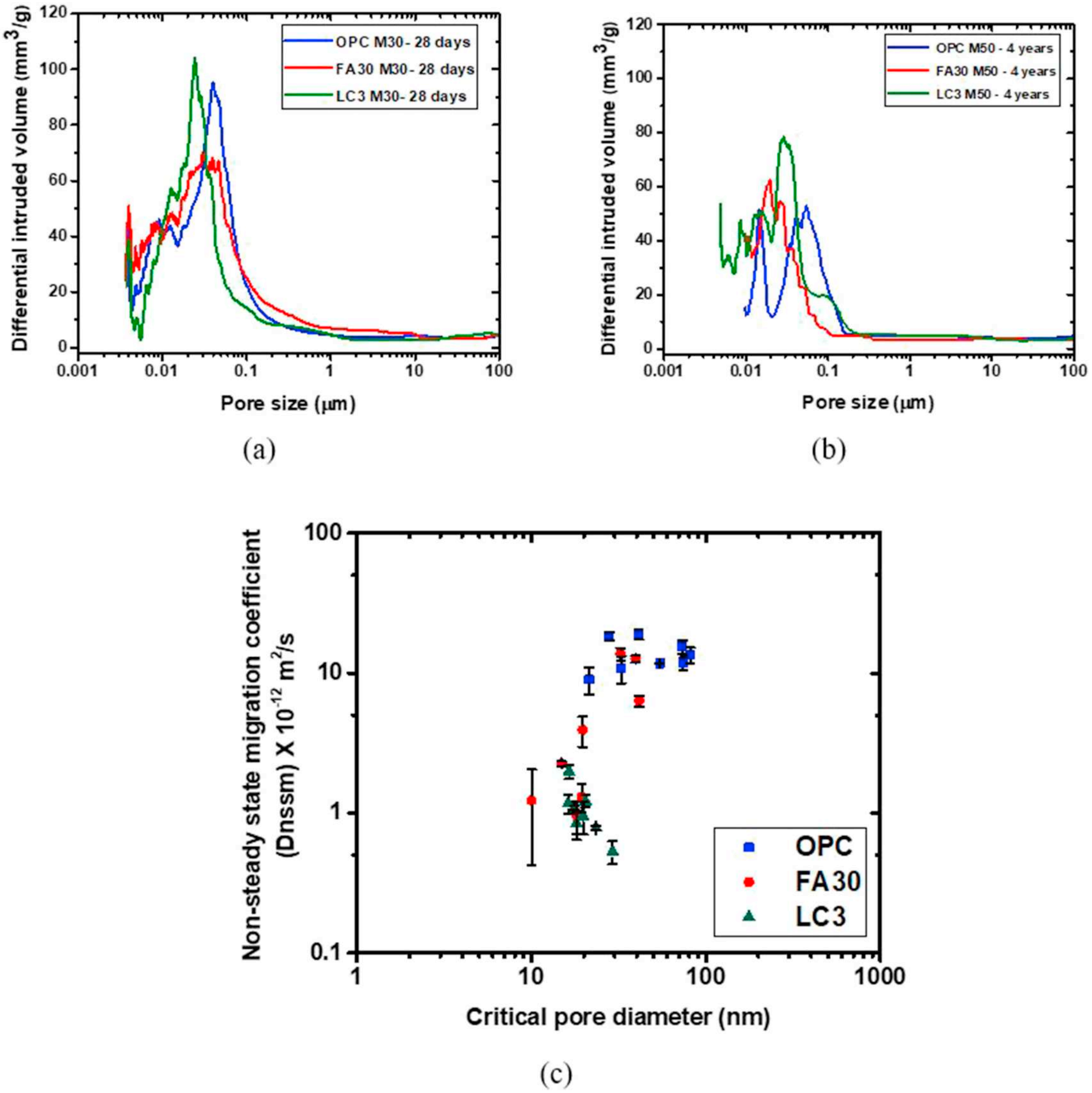

(a)

(b)

(c)

Fig. 10. (a) Pore size distribution in M30 concrete at 28 days, (b) Pore size distribution in M50 concrete at 4 years and (c) dependencies of pore size on the migration coefficient.

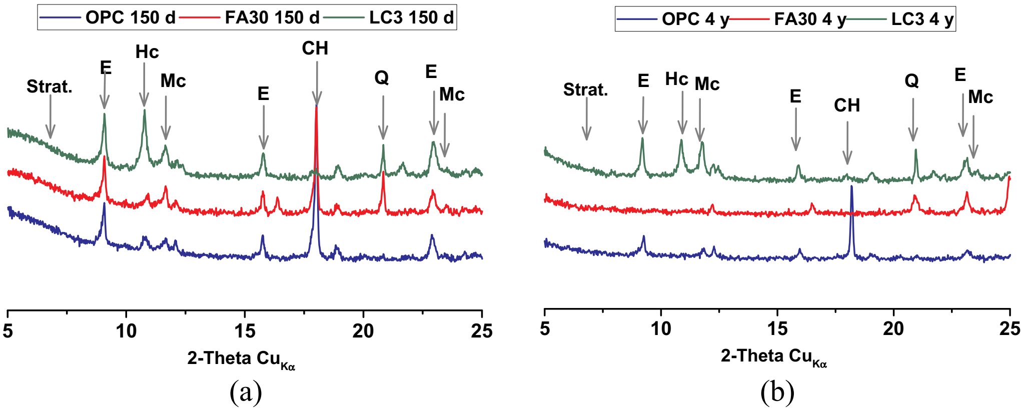

Fig. 11. X-ray diffractograms of hydrated cement paste at 150 days and 4 years.

lower for all calcined clay concretes (in comparison to FA30 systems) due to the rapid development of microstructure in comparison to fly ash based concrete [17]. Ageing coefficient followed an order OPC < LC3 < FA30 in all concrete categorises considered in this study (see Fig. 9). The lower ageing coefficient demonstrates the importance of considering the role of time dependency along with early age benefit in calcined clay binders. The limited change in transport parameter has a direct implication on the long-term service life modelling. The combined effect of initial transport resistance and time dependency needs to carefully be accounted in service life modelling for concrete with calcined clay binder. In a recent study from the authors, the probabilistic estimate showed higher service life despite lower ageing coefficient due to the lower diffusion coefficient obtained initially. The initial early resistance and lower ageing coefficient can have balancing impact on the service life estimation for such binder systems [58]. Hence, the decay in the transport resistance should be assessed for binder systems and carefully chosen in service life modelling as per FIB – 34 [51].

The limitation in the evolution of pore structure due to lack of space for hydration products can place a constraint for the development of transport properties in calcined clay binder (as suggested by [24]) which could limit the evolution of pore structure beyond a certain age. This limitation in the evolution of pore structure results in lower ageing coefficient in calcined clay binders. However, the lack of chemically conducive environment for hydration due to availability of portlandite and alumino-silicate species from SCMs should not be overlooked. The multiplicity in factors necessitates a detailed characterisation of microstructure to identify the driving mechanisms behind limitation in the development of durability parameters in a calcined clay binder system.

4.3. Microstructural characterisation

4.3.1. Pore structure

The pore structure of the hydrated cement matrix in concrete plays a crucial role in the transport parameters. Porosimetry experiments were carried out on M30, M50 and C-mix concrete at 28 and 90 days, and M50 and C-mix concrete at 4 years. Fig. 10 presents typical pore size distribution obtained in M30 concretes for the three binders at 28 days. The pore sizes were similar to the range of values found in cement paste [17,24] which shows that capillary pore size formed within the binding phase remains as the dominant pore size in the concrete system. The pore size of LC3 concretes are found to be shifted to the lower size region. Similar results were found in cement paste made with LC3 binder in previous work from the authors [17]. Fig. 10(b) shows the pore size of M50 grade concretes after 4 years with similar shifted pore structure of FA30 and LC3 systems to plain portland cement. In Fig. 10(c), the variation in migration coefficient and critical pore diameter (both measurements made at 28 days, 90 days and 4 years) shows a considerable dependency of transport parameter based on pore structure alterations. The reduction in the pore sizes is controlled by the reactivity of the ingredients present in the binder, which leads to rapid formation of hydration products. The pore sizes and migration coefficient in LC3 and OPC concretes were found to be concentrated in two different regions (see Fig. 10c) which indicates the key role of binder type, i.e., hydrated phase assemblage formed in a binder type. There is a steady evolution of FA30 concretes to lower migration coefficient, which occurs synonymously with the refinement of pore size, finally reaching a similar range as LC3 concretes. However, pore size evolution is limited about 10–20 nm range for both LC3 and FA30 concretes. Previously, Berodier and Scrivener had shown pore diameter limits close to 12 nm for fly ash and slag binders [24]. In this study, concretes made with different mixture proportioning were also found to reach a similar size range. However, at the narrow range of limiting pore sizes around 20 nm, a major difference in transport parameter between fly ash and LC3 concretes can be noticed. On the other hand, OPC concretes produce nearly similar migration coefficient across a range of pore sizes, as large connected pores can be present at larger pore size range. This scatter reveals that critical pore size alone cannot be the sole premise to rationalise the development of macroscopic properties. The connectivity of pores present in the hydrating matrix should also be further incorporated into the analysis to evolve understanding of the macroscopic impact of the pore size alterations from the composite phase assemblage.

4.3.2. Hydrate assemblage

The composition of the hydrated phase assemblage is influenced by the various interactions of the constituents present in a particular binder system. The use of limestone and calcined clay in conjunction is expected to preserve the ettringite and further, produce additional hydrates phases such as Hemi- (Hc) and Mono-carboaluminates (Mc) [19]. The hydrate phase assemblages of OPC, FA30 and LC3 binders were studied at 150 days and 1400 days of sealed curing. The X-ray diffractograms of LC3 show the distinct presence of Mc and Hc phases (see Fig. 11). The ettringite amount is preserved at 150 days in all the binders due to the presence of limestone (about 5% in the plain portland cement used in control and FA30 binder combinations). Also, traces of carboaluminates were available in OPC and FA30 at 150 days as well. The portlandite (CH) peaks confirm the CH consumption by 150 days because of the high reactivity of calcined clay in LC3 binder. In fly ash binder, the portlandite was found to be limited by 1400 days. Portlandite presence can be seen in OPC at both 150 and 1400 days. The absence of stratlingite form of C-A-S-H can be owing to lower grade calcined clay used in this study.

The quantitative estimates of the phases can be found in Table 3. The total amount of Ettringite, Mc and Hc was found to be about 17% in LC3 binder whereas OPC and FA30 had 9–10% in the overall microstructural composition at 150 days of sealed cured conditions. If the

Table 3
Quantitative phase assemblage of hydration per 100 g of anhydrous binder.

Binder type	Age	C_3S	C_2S	C_4AF	CH	Calcite	Quartz	Ettringite	Mc	Hc	Amorphous
OPC	150d	1.66	7.33	2.74	9.66	1.98	0.86	6.02	2.8	0.92	105.99
FA30	150d	1.05	3.47	1.77	5.53	2.07	5.18	5.56	2.8	0.83	111.44
LC3	150d	2.04	8.42	1.96	1.27	5.68	4.03	7.13	5.71	3.98	99.44

Note: d – days.

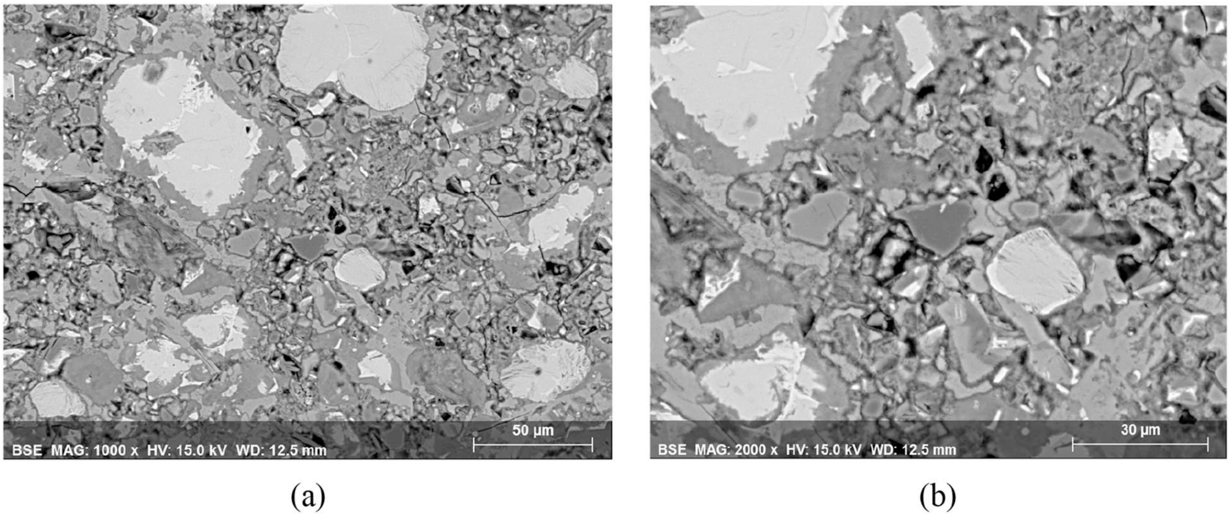

(a) (b)

Fig. 12. Microstructure of OPC at 28 days at two magnifications; a) 1000 X and b) 2000 X; EDX shows a Ca/(Si + Ai) ratio of 1.85 in the C-A-S-H matrix.

molar volume of these phases is taken into consideration, AFm and AFt phases coexist in huge volume in the outer capillary region of the hydrated matrix in LC3 binder which leads to rapid development of the physical structure.

4.3.3. BSE micrographs

Backscattered electron images of the three binders were obtained for hydrated cement paste sealed cured for 28 days. The variation in the micrographs presented at two different magnification levels can provide insights on the localised variation in the microstructure.

Fig. 12 confirms the presence of large portions of anhydrous cement grains, portlandite and large numbers of discrete pores in the hydrated microstructure of plain portland cement. A closer look at the microstructure (see Fig. 12b) shows the compactness and spatial distribution of hydration products in the interparticle capillary pore space. The capillary region plays a dominant role in the durability performance due to the presence of connected pores entangled between porous C-A-S-H, which facilitates transport of ionic species in the concrete media. Both the characteristics of pore network and hydration products present in the outer C-A-S-H control transport properties. In general, the capillary pore space is filled with outer C-A-S-H and other hydrates such as CH, AFt and AFm. The low w/b reduces the free capillary pores because of initial close packing of the binder particles which enables early convergence of hydrated phases in the capillary pore space to produce a dense cementitious matrix. However, the accessibility for external species for transport through concrete is controlled by the chemistry and assemblage of the hydrates formed in the outer C-A-S-H region. The less compact microstructure of the hydrates produced in capillary pore space in OPC systems is the cause for minimal benefit in the transport characteristics of OPC concrete despite reduction in water-binder ratio.

Micrographic evidence of partially reacted and unreacted fly ash particles can be noticed in Fig. 13(a). Also, Fig. 13(b) confirms the absence of large particles of hydration products which give a denser appearance due to pozzolanic hydrates in the capillary pore space. Also, limited signs of large portlandite crystals in the outer C-A-S-H region are seen. At higher magnification, local densification of the cementitious matrix occurs due to deposition of pozzolanic C-A-S-H from fly ash. The chemical composition by EDX confirms the reduced Ca/(Si + Ai) amount in the pozzolanic C-A-S-H as hydrate precipitation is dominated by saturation due to silicate and aluminates species dissolving from SCMs. A vital point to note is the distinct difference in features of the hydrates present in capillary pore space. FA30 shows the prominent presence of finer products, unlike OPC systems.

Fig. 14 presents the micrographs of LC3 systems which reveals a compact microstructure formed due to the combined effects of calcined clay reactivity and space-filling hydrates produced in calcined clay-limestone combination. The composition (Ca/Si + Al) of the C-A-S-H formed in LC3 cementitious systems was reduced to 1.36 compared to 1.85 in OPC system. At higher magnification, a clear indication of the compact cementing matrix in the capillary pore space in the LC3 systems can be noticed (see Fig. 14b). The large phases were identified to be quartz phase present in calcined clay/unreacted part of limestone. Although unreacted phases were present, the space-filling nature of the hydrates was able to produce a compact microstructure. The micrographs strongly support the densified state of hydrates formed in LC3 which has resulted in the reduced pore size (presented earlier in Fig. 10). Also, the reduction in the transport properties barring the effect of the water-binder ratio is due to the high level of compactness of the hydrates formed in capillary space which results in early densification of calcined clay systems. More detailed analysis of the chemistry of the hydrates in inner and outer hydration product can give better insights on the difference in structure formation in these systems.

4.3.4. Characteristics of microstructure

4.3.4.1. Compositional variation in C-A-S-H of OPC, FA30 and LC3 binder:. A compact and denser microstructure formed in LC3 systems confirms the influence of characteristics of hydrates formed in the LC3 cementitious matrix which is driven by the nature of the pozzolanic activity of ingredient and the composite hydrate phase assemblage. In

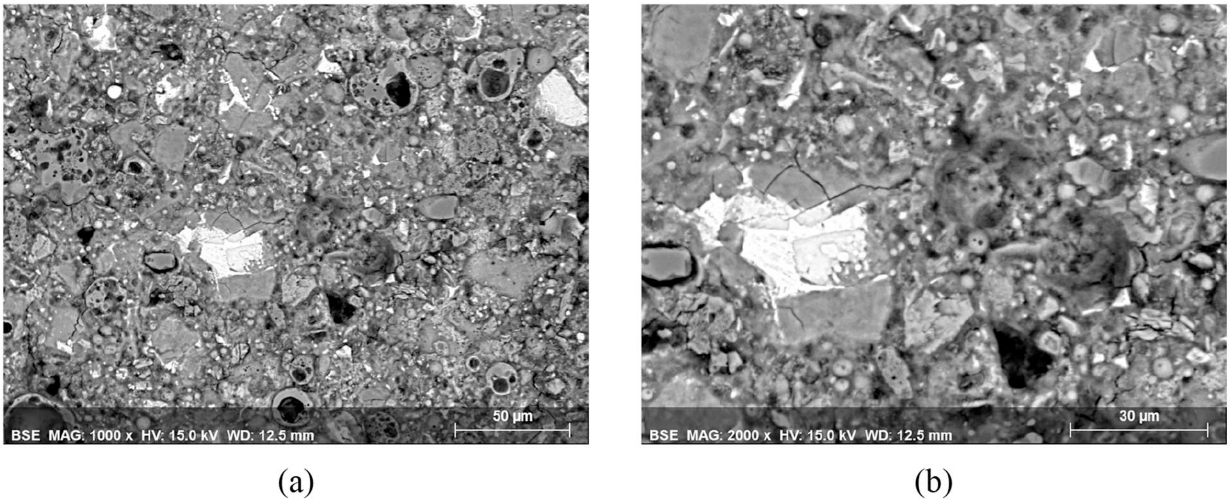

Fig. 13. Microstructure of FA30 at 28 days at two magnifications; a) 1000 X and b) 2000 X; EDX shows a Ca/(Si + Al) ratio of 1.48 in the C-A-S-H matrix.

simple terms, the reactivity of ingredient can be labelled as the driving factor for the microstructural development and plays a crucial role in the development of macro-scale properties. However, the influence of the composite phase assemblage, the kinetics of its build-up and its dynamic contribution to the physical structure should not be neglected. The chemical composition of the microstructure was probed to assess the variation in C-A-S-H composition which can help understand the role of the SCM reactivity on the nature of hydrate formation. The results of EDX analyses of C-A-S-H can be found in Figs. 15 and 17.

The composition of the C-A-S-H produced in OPC, FA30, and LC3 binder systems is presented in Fig. 15. The C-A-S-H in LC3 had a distinctly lower Ca/Si ratio in contrast to the FA30 and OPC. There was a more significant shift in the Ca/Si ratio of FA30 and LC3 systems in comparison to OPC. Also, the C-A-S-H composition indicates greater amount of alumina and silicates in C-A-S-H, more specifically in the LC3 binder system due to the higher reactivity and composition of the amorphous content present in kaolinite clay. The distinct shift in composition is visible due to aluminate availability in the pore solution despite the lower kaolinite content (<60%) in the clay used in these LC3 systems. Previous studies have shown that the alumina incorporation in C-A-S-H was found to be strongly controlled by the availability of alumina rather than Ca/Si ratio of C-A-S-H [59,60].

The characteristic alteration in the chemistry of C-A-S-H has a marked impact on the development of microstructure and in turn, transport parameter in the cementitious systems. Higher reactivity of calcined clay leads to early formation of the low Ca/Si - C-A-S-H which progressively fills capillary pore space with solid hydrates. Also, the low-packing density of C-A-S-H with low Ca/Si ratio increases the macroscopic compactness of solid hydrate deposited in the capillary region. This characteristic carries a direct implication on ionic transport, which depends mainly on the nature and packing of the hydrates present in the capillary region. For instance, all concrete made with LC3 binder tends to show similar build-up of ionic resistance, despite variation in water-binder ratio and concrete mixture proportioning. This distinct performance is controlled by the characteristics of hydration products formed in LC3 binder.

Furthermore, along with pore refinement, the ionic resistance is also affected by the reduction in ionic conduction of the pore solution present in the capillary pore space. Two factors lead to a reduction of ionic conduction: i) consumption of $Ca(OH)_2$ and ii) alkalis binding in the hydrate formed during the pozzolanic reaction. Both these factors collectively result in reduction of pH of the pore solution. The measured pH of pore solution for OPC, FA30 and LC3 binder at 28 days sealed curing was 12.88, 12.72 and 12.32 respectively.

The physical binding of alkalis, which occurs due to adsorption on the surface of pozzolanic C-A-S-H, is analysed from the EDX data. Fig. 16 confirms higher alkali uptake in C-A-S-H (represented as Na + K normalised by Ca/(Si + Al), in terms of atomic ratio). The results

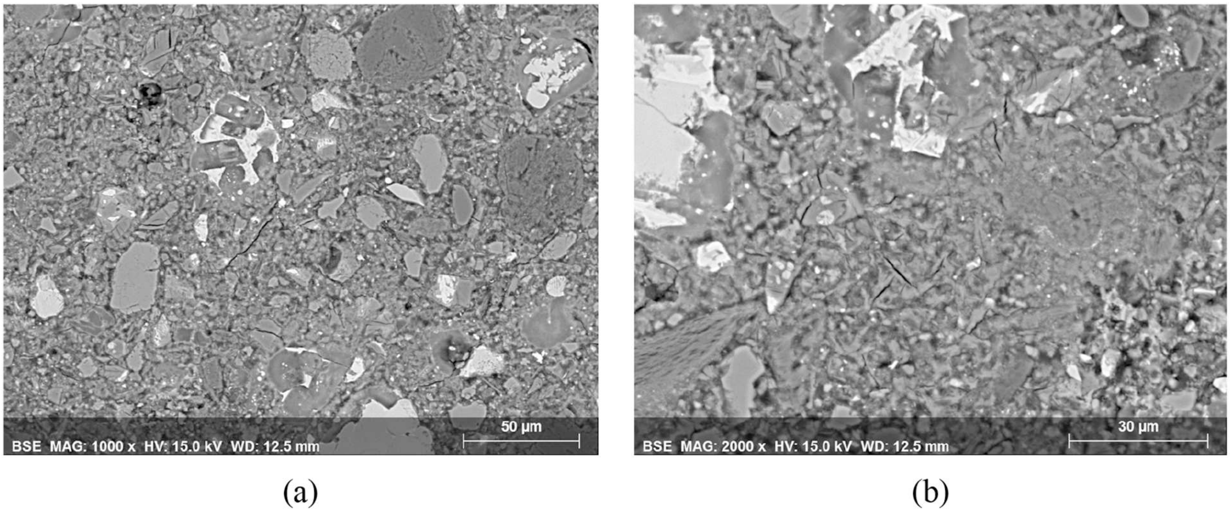

Fig. 14. Microstructure of LC3 at 28 days at two magnifications; a) 1000 X and b) 2000 X; EDX shows a Ca/(Si + Ai) ratio of 1.36 in the C-A-S-H matrix.

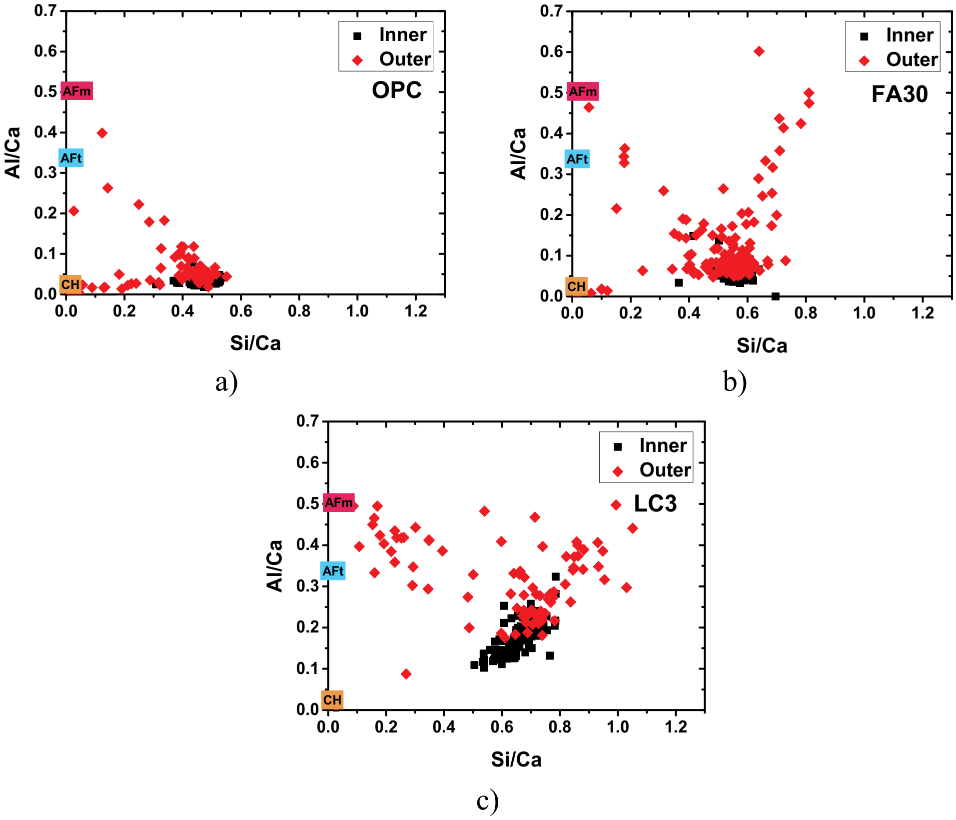

a)

b)

c)

Fig. 15. Composition of the microstructure of C-A-S-H (a), (b), and (c).

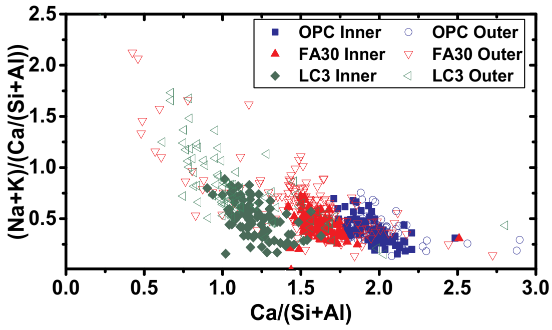

Fig. 16. Alkalis affixed in inner and outer C-A-S-H in OPC (blue), FA30 (red) and LC3 (green). (For interpretation of the references to colour in this figure legend, the reader is referred to the web version of this article.)

indicate that lower Ca content in C-A-S-H tends to create negative surface charges to facilitate alkali uptake. Previously, Hong and Glasser reported the incorporation of alkalis in low Ca/Si- C-S-H based on a study on solid C-S-H with Ca/Si ratio from 0.85 to 1.8 [27]. The difference in alkalis bound in C-S-H and C-A-S-H were found to be insignificant in a recent study by Hopital et al. [61]. Similarly, in this study, significant binding of alkalis was found in the composition of the hydrates present in the outer C-A-S-H region as shown in Fig. 16. Though the composition of the C-A-S-H was shifted towards higher silica and alumina incorporation in the inner C-A-S-H, the change in the amount of the alkali was not markedly altered in the inner product region. More alkalis were present only in the outer products, more specifically in FA30 and LC3 binder. There was no significant variation in the amount of the alkali in the inner and outer product of OPC binder due to higher Ca/Si ratio in both cases for OPC.

In addition to physical structure development, the role of alkali dilution on the early drop in electrical conductivity in the case of calcined clay binder can further escalate the resistance to ionic movement and also alter the transport characteristics as stated in [62]. Consequently, the low mobility state of alkalis in low Ca/Si ratio C-A-S-H can also contribute to ionic resistance against external ions [27]. This aspect of combined pore structure and pore solution effect will be explored in later sections on pore network parameter.

4.3.4.2. Alteration in composition with time:. The change in C-A-S-H composition in the capillary region is more evident due to the pozzolanic reaction which occurs in the presence of the portlandite produced in the capillary region. However, the steady dissolution of silica and alumina can enrich the pore solution with these ionic species and alters the characteristics of hydrate formed at different hydration periods. To reveal the effect of curing time on the composition of pozzolanic hydrate formed, Fig. 17 presents the statistical distribution of the C-A-S-H composition in the inner C-A-S-H region at 28 days and 150 days of curing. There was distinct difference in the composition between OPC, FA30 and LC3 at both ages. The variation due to curing time was found to be insignificant which suggests that intrinsic reactivity state of the SCM controls the composition of microstructure, not merely the curing duration. The dissolution of SCM over time can steadily increase the Si and Al amount for incorporation in C-A-S-H. However, the kinetics of this enrichment is controlled by reactivity or dissolution rate of SCMs which is critical in altering the composition of the hydrate formed in a binder system. Also, a mere increase in curing cannot alter the nature of the C-A-S-H products formed in the microstructure. FA30 concrete evolves slowly, as the fly ash enriches the pore solution slowly over the hydration period and continues to form a similar C-A-S-H due to the low reactivity levels. The high dissolution rate of calcined clay ensures that hydrate formed always has shifted chemical composition, i.e., lower Ca/Si ratio. The characteristics of the LD pozzolanic C-A-S-H and impact on the physical structure also draws a connection to the early reactivity of

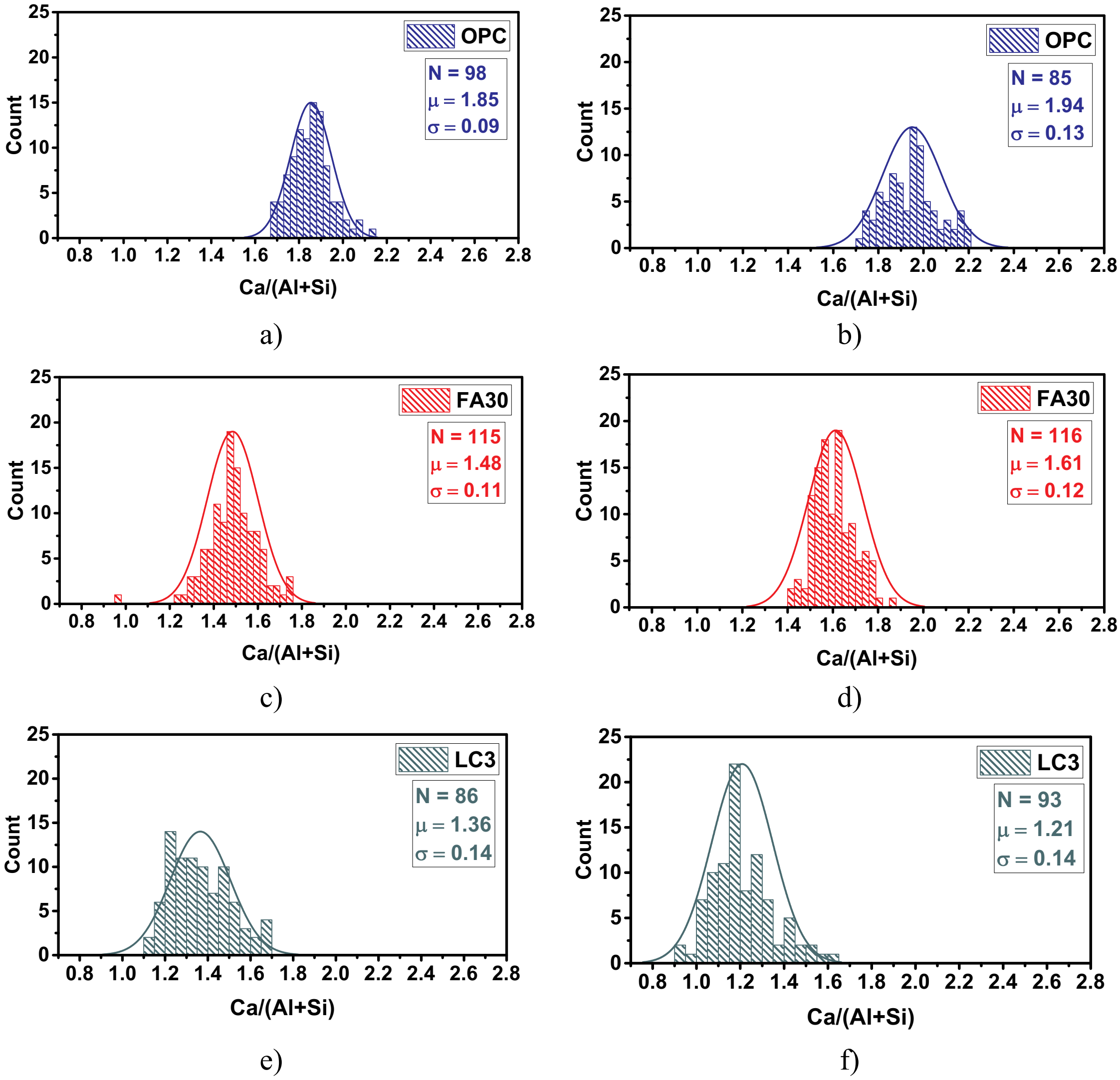

a) b) c) d) e) f)

Fig. 17. Distribution of C-A-S-H composition for 28 days cured (a), (c) and (e) and 150 days cured (b), (d) and (f) pastes.

calcined clay, its effect on microstructural development and the corresponding early impact on the macroscopic properties.

4.3.4.3. Physical characteristics of C-A-S-H formed in OPC, FA30 and LC3 binder:. The difference in phase assemblage and the variations in the chemical composition of the major hydrate phase, i.e., C-A-S-H, need to be characterised for probing the role of hydrates formed in LC3. Studies based on the indentation modulus have previously categorised the C-A-S-H as HD(high density)-C-A-S-H and LD(low density)-C-A-S-H based on stiffness values and packing density of C-A-S-H (i.e., solid packing fractions) [63–65]. Based on the micro-stiffness, the packing density and volume filling potential due to alteration in the composition of the hydrate phase can be indirectly probed. Most importantly, the distribution of the individual governing phase in terms of average modulus and volume fraction of the different hydrates can also give new insights on the complex LC3 binder system. Due to the multiplicity of the interactions between different components in the microstructure of blended systems, the phases are dispersed over different regions of moduli. The C-A-S-H formed from clinker dissolution is dominant in the microstructure of OPC, and C-A-S-H formed due to pozzolanic reaction is dominant in the microstructure of FA30 and LC3 can explain the underlying difference in the contribution of interactions in these systems.

For a detailed understanding of the dominant moduli in the microstructure, multipeak deconvolution was carried out in Origin Pro 2016. The entire frequency distribution of the modulus was categorised in terms of different regions based on the variation in distribution. At every peak position, the gaussian function was controlled in terms of peak position or centroid of the distribution, the area and full width at half maximum (FWHM). All these parameters were iteratively reduced by minimisation of the least square error to collectively produce the experimental curve. The goodness of the fit was classified in terms of goodness of fit and R^2 value.

The peak position of the individual Gaussian curve indicates the representative value of the dominant modulus region. The area of the curve can represent volume fraction of the phase, and FWHM can give some indication of the concentration of the dominant modulus or dispersion in the dominant moduli obtained. These parameters can give important information on the nature of the hydration product formed, the process of formation and interference of the pozzolanic reaction on the hydrates formed.

Fig. 18 presents the deconvoluted probability densities along with the experimental response and confirms a consistent reproduction of the cumulative deconvoluted peak and experimental peak for all three binder systems, which validates the analysis scheme. The indentation modulus positions of the OPC show a major modulus region concentrated around 30 GPa, harmonious with the value reported in literature for OPC [66]. Also, other moduli were found to be concentrated

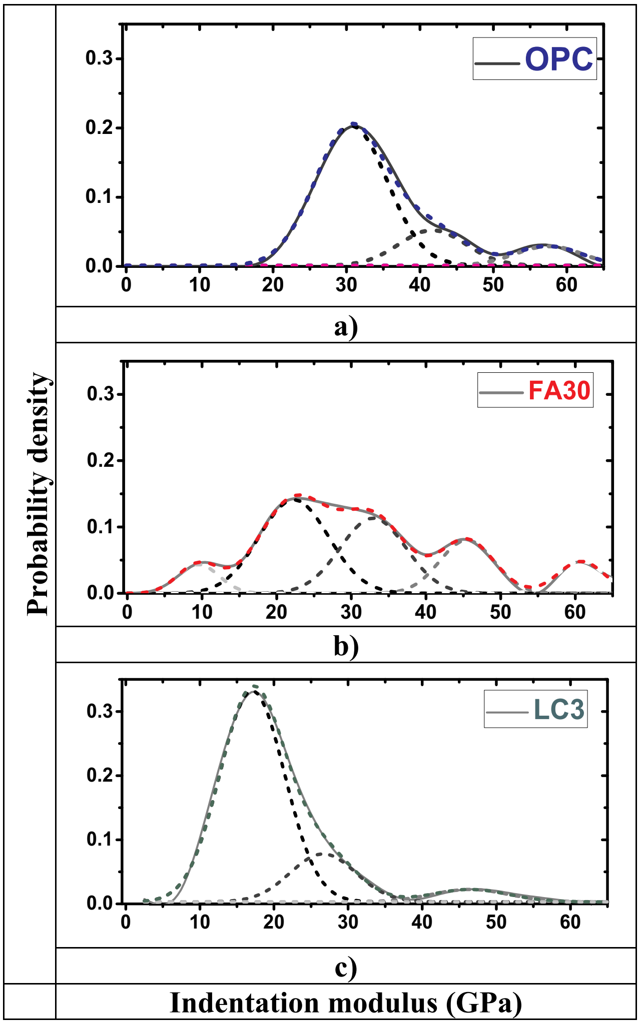

Fig. 18. Micro-mechanical characteristics of microstructure formed in a) OPC, b) FA30 and c) LC3 at 150 days.

around 45 GPa corresponding to intermixed C-A-S-H and CH region, and about 55 GPa for the CH dominant region. Notably, all values of the modulus were above 20 GPa in OPC.

On the contrary, FA30 had moduli in two additional regions in addition to the major three regions seen in OPC. A significant portion of moduli was concentrated around 20 GPa or below due to the reduced Ca/Si ratio in the pozzolanic C-A-S-H in the FA30 binder phase. The moduli value is reduced further for LC3 binder in correspondence with the lower Ca/Si ratio in comparison to OPC and FA30 binder. Collectively, the portion and proportion of the low modulus C-A-S-H formed in these systems confirm the formation of low-packing density states, which is the driving cause for the significant change in physical structure development in LC3 binder.

4.3.5. *Pore network parameter: tortuosity*

Tortuosity is characteristic of pore connectivity and can be considered as a representative pore network parameter for cement-based materials. A summary of the electrical tortuosity (based on Eq. (2)) for the different concrete across the moist curing period is presented in Table 4. The pore solution conductivity (based on Eqs. (3) and (4)) was analysed only at 28 days, and after that, the changes were considered to remain insignificant. The value of pore solution conductivity obtained for OPC in this study is similar to the reported value for the OPC system at 0.5 w/b ratio in [54,67]. In [67], it is also reported the value does not change beyond 24 h.

Table 4
Summary of pore solution conductivity value and estimated electrical tortuosity.

Mix I.D.	Concrete grade	Pore solution conductivity	Tortuosity	Tortuosity	Tortuosity
		S/m	28 days	90 days	365 days
OPC	M30	5.17	5.75	6.67	9.65
	M50		5.73	6.68	7.75
	C-Mix		5.89	6.05	7.53
FA30	M30	3.74	7.43	11.82	17.10
	M50		7.42	11.35	17.29
	C-Mix		5.75	5.69	10.34
LC3	M30	1.43	14.87	18.97	27.93
	M50		12.13	19.50	26.06
	C-Mix		16.49	21.07	29.26

The tortuosity values of OPC concrete reported in this study were between 5 and 8 across different ages which is similar to the values reported in Yang et al. [37] for OPC systems. Also, the reduction in tortuosity value of OPC was minimal post early curing period. In contrast, the tortuosity value of FA30 concrete improved drastically after 28 days. At 28 days, tortuosity was only marginally higher for all FA30 concrete with respect to OPC concretes. However, the value increased dramatically, nearly twice, by 365 days due to continued influence of pozzolanic hydrates produced from fly ash. LC3 concretes attained higher tortuosity values by 28 days, which indicates that increased disconnectedness in porosity occurs in direct correspondence with the reduction in pore size as observed in LC3 binder. In a multi-component binder system, the tortuous nature of the porous structure is a direct measure of the influence of the diverse phase assemblage. Also, the contribution of the pozzolanic gel to the transport parameter is captured by pore network parameter which reflects as higher tortuosity for all LC3 concretes than OPC and FA30 concretes across the curing period.

4.3.6. *Interpretation of the role of microstructure parameters on transport properties*

As ionic transport is intrinsically dependant on the nature of pore network, the relationship between transport phenomenon and tortuous nature of pores was explored based on formulations in literature [68,69] (see Eq. (6)). An explicit dependence of the chloride resistance on the tortuous nature of the pore structure was identified in correspondence with the diffusional tortuosity (see Fig. 19). The electrical tortuosity deals with the tracer path for transport of a charged electron with respect to the relative conductivities of pore solution and concrete bulk system. Diffusional tortuosity relates to relative diffusivities for

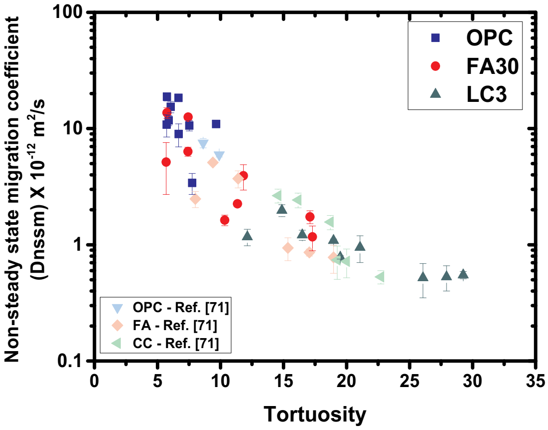

Fig. 19. Relationship between non-steady state migration coefficient and tortuosity.

movement of ions which are much larger in atomic size compared to an electron. From Nernst-Einstein equation, the diffusion of ions in a charged medium is proportional to the conductivity of the solution available for transport of ions in bulk systems (see Eq. (7)). Here, D_o is the diffusion coefficient of the Cl^- ion at infinite dilution, equal to 20.3×10^{-10} m^2/s [68,70], D_0 is known as self-diffusion coefficient of an ion at a particular temperature, i.e., the diffusion coefficient through the infinitely dilute pore solution, ϕ is the porosity, and τ is tortuosity of the pore system.

$$D_{eff} = \frac{\phi}{\tau^2}.\, D_{inf} \tag{6}$$

$$\frac{D_{eff}}{D_o} = \frac{\sigma_{eff}}{\sigma_o} = \frac{\phi}{\tau^2} = \frac{1}{F} = \phi.\, \beta \tag{7}$$

Fig. 19 shows the influence of tortuosity as a pore network parameter of concrete systems to explain chloride transport. Additional data from [71] from a different study with binary and ternary concretes (400 kg/m^3 binder content and 0.4 w/b ratio) with fly ash (FA) and calcined clay (CC) along involving limestone and quartz powder was used to reinforce the credibility of the proposed relationship to capture the behaviour of ternary concrete systems. See Annexure 1 for summary of data used in tortuosity-D_{nssm} relationship. The trends suggest that both reduction in porosity and tortuosity leads to improved transport resistance. The change in porosity levels of the concretes leads to spread in chloride penetrability-tortuosity relationship. As fly ash concretes reach similar tortuosity levels either by reducing porosity by mixture proportioning or extended curing, it can reach similar the chloride penetrability resistance.

In order to break down the influence of tortuosity on chloride transport and decouple the role of pore structure evolution and pore solution, the sensitivity analysis of tortuosity estimate for different dependent parameters was performed. Fig. 20 presents the effect of the change in conductivity of pore solution to emphasise on the sensitivity of the tortuosity estimates. For the sensitivity analysis, the mean value of 7.45, 4.25 and 10 were considered for electrical conductivity, pore solution conductivity and porosity respectively, which corresponds to a tortuosity value of 7.55, close to the OPC value. Then, individual parameters were varied by controlling the other two parameters to be constant. The experimental limits obtained in the nine concretes were used to fix the boundary values for the analysis. For instance, electrical conductivity value was varied from 15 mS/m to 0.1 mS/m, and porosity was varied from 10% to 1.5%. The range set for pore solution conductivity was 10 S/m to 1.5 S/m. From Fig. 20(a), for a constant bulk conductivity and pore solution conductivity, tortuosity increases with increase in porosity based on Eq. (1). Also, the extent of variation in tortuosity due to porosity and pore solution (Psc) was limited in comparison to changes in electrical conductivity (Ec).

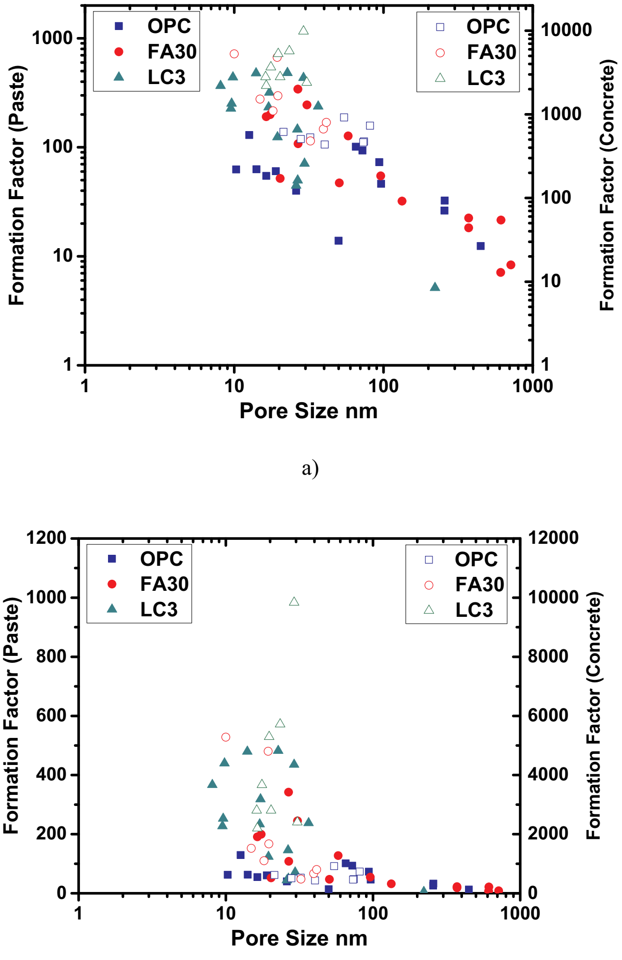

a)

b)

Fig. 21. Pore size governing the structure development and transport parameter. Data set details: 9 concretes from Phase-1 at 28 days,90 days and 5 concretes at 1400 days. Cement paste with three water-binder ratios for three binders at five ages unto 90 days – MIP was carried out on random samples for each binder type at a different age to cover sufficient samples at an early age and later age for all three binder types. a) and b) is presented separately to distinguish the two regimes; a) shows initial marginally rise in formation factor with pore size (regime 1) and b) shows densification regime with significant rise formation factor in the limiting critical pore size (regime 2).

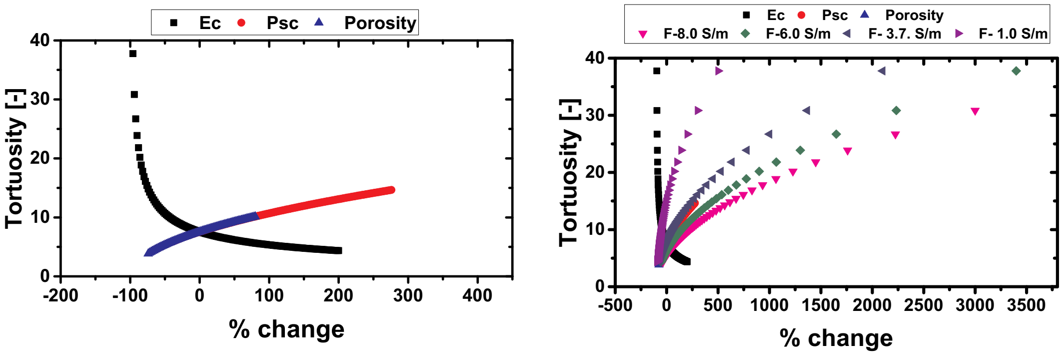

a)

b)

Fig. 20. Sensitivity of tortuosity estimates to changes in porosity, pore solution conductivity and bulk electrical conductivity. a) Tortuosity impacts based on the dependant parameters, and b) change in tortuosity for same structure evolving with different pore solutions.

In Fig. 20(b), the change in formation factor with three different pore solution conductivity values is shown to bifurcate the combined influence of the pore structure and pore solution on the tortuosity. The change in the profile of tortuosity for different pore solution conductivity indicates the consequence of the reduction in ionic strength of pore solution on the tortuosity value. An order of magnitude drop in resistance to chloride ingress in LC3 systems should be attributed to combined contribution from the reduction of pore connectivity and ionic strength of pore solution due to dilution and alkalis binding. Also, the formation of pozzolanic C-A-S-H leads to a reduction of pore connectivity as well as dilution of alkalis. Hence, both the factors collectively lead to higher resistance to ingress of external ions.

4.4. Perspectives on structure development and proposed mechanism

A combined reduction in pore connectivity and porosity leads to a rise in formation factor. In order to identify the role of pore sizes on evolving pore connectivity, Fig. 21 presents the change in formation factor for the concretes and cement paste with the critical pore sizes at the corresponding age of testing. Additionally, formation factor and pore sizes reported in [17] on cement paste were also combined with the results obtained in this study.

The formation factor improves as a function of pore size. As critical pore size reduces, the formation factor increases correspondingly. However, a major rise in concrete properties was found to occur once the concrete has reached a critical pore size of around 10–30 nm. Previously a study by Beroider et al. [24] and Avet et al. [11] report that pore sizes reaches a limiting value and does not evolve continuously. A critical extension to the understanding is presented in this study which showcases that once a limiting pore size is attained in capillary pore space, there is a significant rise in formation factor, which is indicative of better macroscopic performance parameters such as chloride diffusion rate. This increase suggests that once a critical pore size is reached, the capillary porosity reduction occurs in the larger pores to bring the pore size to similar critical size in other regions. During this process the critical pore size does not reduce significantly; however, the volume of pores in the larger pore size reduces and these pores start lowering to the nearly similar critical pore size range.

Based on the rise in macroscopic physical characteristics (i.e., formation factor), a two-fold structure development mechanism to conceptualise microstructural evolution in cement composites can be put forward. Initially, the convergence of hydrates in the capillary pore space occurs to reduce pore structure up to a critical size range (regime 1), which is followed by the densification of physical space in the microstructure (regime 2). The extent of densification (i.e., shoot up in regime-2 with a rise in formation factor) in calcined clay and fly ash composites brings out the role of driving potential (i.e., the reactivity of the SCMs) which governs the presence of conducive chemical species to continue the formation of hydration products. This chemical driving potential leads to precipitation in the interim pore space and densifies the capillary region of the cementing matrix. The lack of driving force limits the rise in formation factor for OPC binder while fly ash and calcined clay could create conditions for an extended structure development due to availability of chemical species to cause precipitation of pozzolanic C-A-S-H in the finer pores. At a macroscopic scale, this phenomenon leads to high ageing coefficient in the blended binder in comparison to plain portland cement systems. Previously, Durdzinski et al. [72] proposed a bi-linear relationship between strength and gel space ratio relationship and attributed the second regime to the densification of the matrix. In this study, the densification is associated with the rise in physical structure parameter (i.e., formation factor) at critical pore size. Further, this understanding can explain the dramatic increase in the formation factor in some binder compositions and bifurcate the contributions from SCMs and limestone fillers in ternary cement composites.

$$\frac{1}{r} = \frac{R.\,T}{2\gamma V_m}.\,\ln(10^{SI}) \tag{8}$$

Fig. 22 presents the role of pore size on formation factor of the concrete systems alone. The saturation levels required for the precipitation of different phases are shown in Fig. 22b based on the Oswald Freundlich formula stated in Eq. (8) [73,74]. This relationship confirms that as the pore size reaches a critical range, the supersaturation to cause precipitation in these finer pores increases. Henceforth, the available chemical species in pore solution will not be sufficient to cause further hydrate formation in the pore space [74]. The hydrate precipitation depends upon conducive chemical species and equilibrium of solid-pore solution which leads to formation of hydrates in the finer pores or the larger interim space, if available. The driving force to form a hydration product in finer pores will be higher, which is sustained by high reactivity potential of calcined clay. Hence, the shift in the pore size occurs more rapidly in the case of calcined clay binder. Once the pore size reaches a critical size, then precipitation start occurs in the available larger interim spaces which causes a dramatic rise in formation factor due to the hydrate formation in the interim space which leads to the disconnectedness of the porosity, i.e., increase in tortuous nature of the pore network during this phenomenon.

Fig. 22b gives the theoretical relationship between saturation index (SI) and pore radius for three phases, i.e., C-S-H, AFt and Hc based on the molar volume of the hydrate phase at constant interfacial energy [73]. There is a constraint or limitation on the hydrated phases with higher molar volume, i.e., AFt and Hc. The lack of large pores to accommodate these phases results in limited growth of these phases. As the pore size reduces, precipitation of these phases will be inhibited at lower concentration and ions will start getting accommodated in the C-A-S-H which can cause much easy precipitation in the finer pores at lower saturation index as shown by [73]. This results in slowing down of the evolution in the calcined clay binder, i.e., reduced ageing coefficient for all concrete made with a calcined clay binder. Despite the smaller pore size in LC3 binder, the rise is formation factor is sustained due to ability of the chemical species to cause precipitation of low Ca/Si C-A-S-H in the available interim space in the capillary porosity. This rise in formation factor signifies further reduction in the volume of pores by filling the larger pores and brings them to nearly same critical pore size range. Since chemical species from the SCM play a critical role in saturating the pore solution with soluble ions (i.e., aluminates and silicates) to precipitate pozzolanic gel, the choice of SCMs is primary governing factor which can drive the precipitation in the finer pores. This mechanism explains the reasoning behind the choice of binder being the dominant factor for the systematic development of properties at a range of water-binder ratios and concrete mixture proportions with LC3 and FA30. The physical structure development of concrete systems is strongly controlled by the kinetics of microstructural evolution in the binding matrix. The physical difference of microstructure between 1 day and 28 days is presented in Fig. 23 for the three-binder types reported in this study. The direct relevance of the kinetics of resistivity development in paste and concrete indicates that more complex binding mixtures can be designed, or tailor-made based the underlying knowledge on structural development in cementitious paste.

Fig. 24 presents a representation of critical information on the characteristics of physical structure development. The schematic represents a critical viewpoint of the structure development at later age and impacts on property development based on the experimental observations made in this study.

i. Fig. 24a denotes that the porous outer C-A-S-H spreads to reduce the interparticle space of the solid species as shown by the conductivity data across different w/b.
ii. Fig. 24b denotes the formation of inner C-A-S-H along with progressive deposition of hydrates in the capillary region
iii. Fig. 24c indicates that the pore size reaches a critical size range.

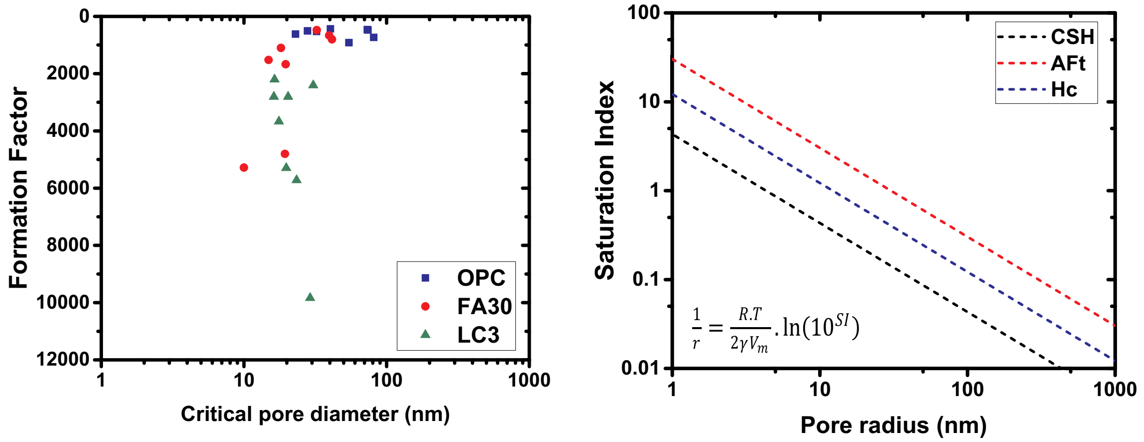

(a) (b)

Fig. 22. (a) Limiting pore size to attain densification, and (b) saturation level required for precipitation of C-S-H, AF_t and Hc at different pore sizes.

After reaching the critical pore size, precipitation starts occurring in other larger interim spaces of the existing hydrate. At this stage, the pores start to get disconnected. This phenomenon occurs rapidly in more reactive pozzolans due to precipitation of low Ca/Si – C-A-S-H, as saturation index of CSH can be dominated by release rate of silicate and aluminates from SCMs.

iv. Fig. 24d denotes the formation of low Ca/Si CSH, which forms in the finer pore spaces and densifies the cementing matrix. At critical pore size range, significant depercolation of capillary pores occurs which makes the pore network tortuous. During this densification regime, there is a significant improvement in the transport parameter.

v. Furthermore, more alkalis are bound in pozzolanic CSH as denoted in Fig. 24c. Thus, lower alkali concentration in pore solution reduces the diffusivity of external ion due to restricted ion exchange process. This phenomenon also contributes to higher ionic resistance in binders with varying chemistry in addition to pore refinement.

5. Conclusion and perspectives

In this study, the performance evaluation of limestone calcined clay cement with respect to strength development and durability characteristics, with a focus on the role of microstructure was elucidated. Specific conclusions based on the range of different properties of paste and concrete investigated are as follows:

i. An early contribution of calcined clay to strength and resistivity development occurs across a range of water-binder ratio. The role of SCM in composite binder affects electrical conductivity measurements more significantly than mechanical characteristics, which are dominated by initial w/b.

ii. Chloride resistance of concretes in a range of different binder chemistries can be explained by the formation factor approach.

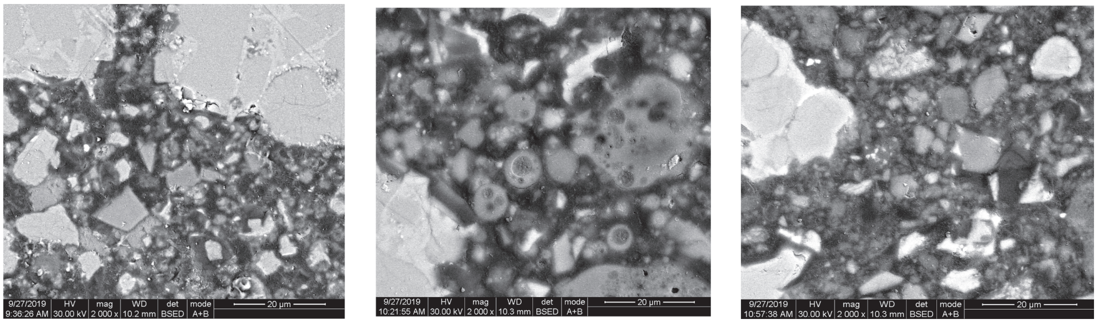

OPC 1 day FA30 1 day LC3 1 day

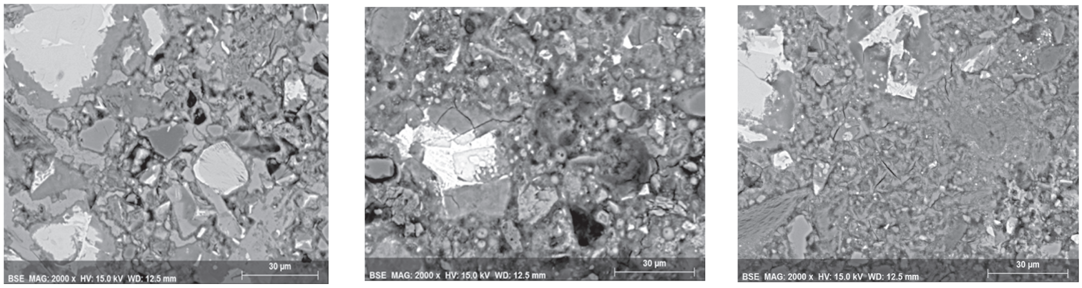

OPC 28 days FA30 28 days LC3 28 days

Fig. 23. Difference in the capillary pore space captured by micrographs at 1 day and 28 days for OPC, FA30 and LC3. 1-day micrographs show the extent of connected porosity in all system and the difference between the binder system is visible by 28 days.

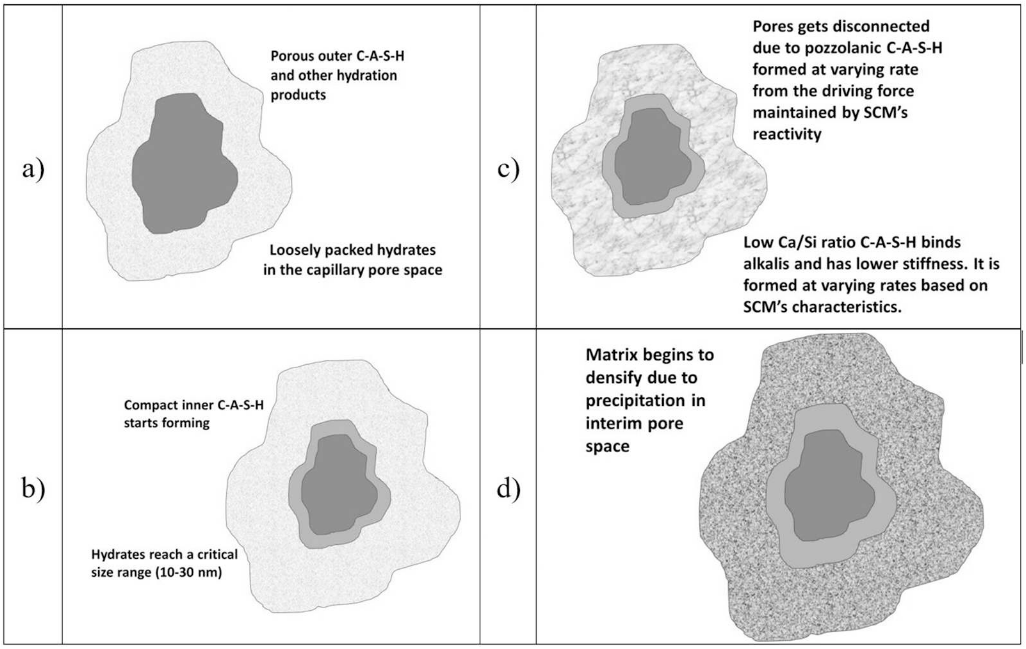

Fig. 24. Schematic of conceptualisation of the microstructure development of hydrates present in capillary pore space. a) presents formation of porous outer C-A-S-H at early ages, b) represents formation of inner C-A-S-H and increase in the amount of outer C-A-S-H, c) presents the beginning of the pozzolanic C-A-S-H causing densification the matrix with LD-C-A-S-H containing alkalis and d) shows the densified matrix with significant precipitation in the interim space.

Formation factor was found to be distinctly indicative of physical structure development and transport properties. Early and later age resistivity of LC3 concrete systems was an order of magnitude higher than OPC concrete.

iii. Time-dependent change in chloride parameters is critical to understand long term contribution during the service of the concrete structure. Ageing coefficient of calcined clay binder was consistently lower than for fly ash concrete across water-binder ratios. The importance of combined characterisation of initial transport and time-dependent change is crucial to compare binder systems. Electrical measurement can give a reasonable assessment of ageing coefficient.

iv. Chloride transport is strongly controlled by the pore structure of the binder phase. Calcined clay-limestone binder produces a unique phase assemblage with a significant amount of AFm (carboaluminate) phase present at a later age, i.e., 150 days and 4 years. These phases along with pozzolanic C-A-S-H from calcined clay lead to a dense microstructure. The reduction in stiffness due to lower packing density of C-A-S-H and alkali binding of C-A-S-H produced in calcined clay is significant in comparison to pozzolanic C-A-S-H in fly ash.

v. Tortuosity as a pore network parameter is a suitable measure to account for the combined effect of pore refinement and pore solution composition to explain the chloride transport under a generalised framework. LC3 systems attain significantly higher tortuosity state at an early age in comparison to FA30 systems.

vi. A structural development mechanism to conceptualise microstructural evolution in cement composites is presented which is based on i) convergence of hydrates in the capillary pore space to reduce pore structure up to a critical size range, and ii) densification of physical space in the microstructure. The extent of densification in calcined clay and fly ash composites bring out the role of driving potential (i.e., the reactivity of the SCMs) which governs the presence of conducive chemical species to sustain the formation of hydration products in finer pores. Refinement of pore size alone does not indicate the physical structure development of concrete microstructure which occurs beyond a critical pore size range.

vii. Densification of capillary porosity occurs once physical space becomes constrained for further precipitation at about 10–30 nm. During this densification regime, pores become largely disconnected and tortuous. Low reactivity SCMs such as fly ash takes a longer time to build up the concentrations in pore solution for higher saturation to cause precipitation in finer pores.

Declaration of competing interest

The authors declare that they have no known competing financial interests or personal relationships that could have appeared to influence the work reported in this paper.

Acknowledgements

The authors would like to acknowledge the financial support from the Swiss Agency for Development and Cooperation (SDC) (Project number: 7F-08527.02.01) for the study. Department of Science and Technology and Funds for Improvement of Science and Technology (FIST) Infrastructure grants from the Government of India are also gratefully acknowledged. Prof. K. Scrivener, EPFL, Lausanne, Switzerland is acknowledged for the access to SEM facilities used for EDX analysis reported in this study. Prof. Narayanan Neithalath, ASU is also gratefully acknowledged for fruitful discussions.

Appendix 1. Annexure

Summary of data used in Dnssm Vs Tortuosity relationship.

Binder type.	Concrete details	Porosity %			Non-steady state migration coefficient (Dnssm) × 10^{-12} m^2/s			Formation Factor		
		28 days	90 days	365 days	28 days	90 days	365 days	28 days	90 days	365 days
OPC	M30	7.6	8.8		18.82	18.36	10.94	435.55	507.36	1061.60
	M50	6.2	7.2		10.81	8.96	3.41	528.08	616.94	829.85
	C-Mix	7.3	7.9		11.75	15.39	10.62	474.31	461.60	715.07
FA30	M30	8.3	8.4		12.55	3.96	1.74	666.66	1669.64	3495.32
	M50	6.9	8.5		6.34	2.25	1.17	800.85	1520.32	3528.30
	C-Mix	6.9	2.9		13.66	5.14	1.63	480.10	1100.00	3631.06
LC3	M30	8.3	9.8		1.97	1.08	0.53	2200.00	3666.67	7944.44
	M50	5.2	6.6		1.17	0.78	0.52	2803.92	5720.00	10,214.29
	C-Mix	9.7	8.4		1.21	0.94	0.55	2803.92	5296.29	10,214.29
Data used from A. Poshnath's work [71]										
OPC		9.04		6.69	7.52		5.95	822.4		1466.36
Fly ash mixes	FA30 (70%OPC + 30%FA)	10.45		4.63	3.71		0.86	1244		6276.76
	FA30L15 (55%OPC + 30%FA +15Limestone)	9.56		5.5	2.48		0.94	670.4		4280.32
	FA30Q15 (55%OPC + 30%FA +15Quartz)	9.58		7.37	5.11		0.78	921.9		4882.37
Calcined clay mixes	CC30 (70%OPC + 30%CC)	9.27		4.67	1.57		0.53	3777.8		11,051.41
	CC30L15 (55%OPC + 30%CC +15Limestone)	11.95		5.32	2.43		0.74	2185.2		6972.50
	CC30Q15 (55%OPC + 30%CC +15Quartz)	9.11		4.34	2.65		0.72	2328.9		9221.14

References

[1] WBCSD, IEA, Technology Roadmap: Low-carbon Transition in the Cement Industry, (2018), https://doi.org/10.1007/SpringerReference_7300.

[2] WBCSD, IEA, Cement technology roadmap 2009: carbon emissions reductions up to 2050, Cem. Sustain. Initiat. World Bus. Counc. Sustain. Dev, 36 2009 (doi:978-3-940388-47-6).

[3] C. Shi, B. Qu, J.L. Provis, Recent progress in low-carbon binders, Cem. Concr. Res. 122 (2019) 227–250, https://doi.org/10.1016/j.cemconres.2019.05.009.

[4] E. Gartner, T. Shi, Alternative cement clinkers, Cem. Concr. Res. 114 (2018) 27–39, https://doi.org/10.1016/j.cemconres.2017.02.002.

[5] S.A. Miller, V.M. John, S.A. Pacca, A. Horvath, Carbon dioxide reduction potential in the global cement industry by 2050, Cem. Concr. Res. (2017) 0–1, https://doi.org/10.1016/j.cemconres.2017.08.026.

[6] M.C.G. Juenger, F. Winnefeld, J.L. Provis, J.H. Ideker, Advances in alternative cementitious binders, Cem. Concr. Res. 41 (2011) 1232–1243, https://doi.org/10.1016/j.cemconres.2010.11.012.

[7] K.L. Scrivener, V.M. John, E.M. Gartner, Eco-efficient cements: potential, economically viable solutions for a low-CO_2, cement- based materials industry, United Nations Environ. Program. Paris. (2017) 1–64 http://hdl.handle.net/20.500.11822/25281.

[8] K. Scrivener, F. Martirena, S. Bishnoi, S. Maity, Calcined clay limestone cements (LC3), Cem. Concr. Res. (2017) 1–22, https://doi.org/10.1016/j.cemconres.2017.08.017.

[9] V.M. John, B.L. Damineli, M. Quattrone, R.G. Pileggi, Fillers in cementitious materials — experience, recent advances and future potential, Cem. Concr. Res. (2018), https://doi.org/10.1016/j.cemconres.2017.09.013.

[10] K.L. Scrivener, Options for the future of cements, Indian Concr. J. 88 (2014) 11–21.

[11] F. Avet, K. Scrivener, Investigation of the calcined kaolinite content on the hydration of Limestone Calcined Clay Cement (LC3), Cem. Concr. Res. 107 (2018) 124–135.

[12] S. Krishnan, S. Bishnoi, Understanding the hydration of dolomite in cementitious systems with reactive aluminosilicates such as calcined clay, Cem. Concr. Res. 108 (2018) 116–128, https://doi.org/10.1016/j.cemconres.2018.03.010.

[13] S. Krishnan, S.K. Kanaujia, S. Mithia, S. Bishnoi, Hydration kinetics and mechanisms of carbonates from stone wastes in ternary blends with calcined clay, Constr. Build. Mater. 164 (2018) 265–274, https://doi.org/10.1016/j.conbuildmat.2017.12.240.

[14] R. Gettu, A. Patel, V. Rathi, S. Prakasan, A. Basavaraj S., S. Palaniappan, Influence of incorporating supplementary Cementitious materials on the sustainability parameters of cements and concrete in the Indian context, Mater. Struct. 5 (2019). doi:https://doi.org/10.1617/s11527-019-1321-5.

[15] Y. Dhandapani, T. Sakthivel, M. Santhanam, R. Gettu, R.G. Pillai, Mechanical properties and durability performance of concretes with Limestone Calcined Clay Cement (LC3), Cem. Concr. Res. 107 (2018) 136–151, https://doi.org/10.1016/j.cemconres.2018.02.005.

[16] M. Santhanam, Y. Dhandapani, R. Gettu, R. Pillai, Perspectives on durability of blended systems with calcined clay and limestone, Calcined Clays Sustain. Concr. Proc. 3nd Int. Conf. Calcined Clays Sustain. Concr, 2019.

[17] Y. Dhandapani, M. Santhanam, Assessment of pore structure evolution in the limestone calcined clay cementitious system and its implications for performance, Cem. Concr. Compos. 84 (2017) 36–47, https://doi.org/10.1016/j.cemconcomp.2017.08.012.

[18] F. Avet, E. Boehm-Courjault, K. Scrivener, Investigation of C-A-S-H composition, morphology and density in Limestone Calcined Clay Cement (LC3), Cem. Concr. Res. 115 (2019) 70–79, https://doi.org/10.1016/j.cemconres.2018.10.011.

[19] T. Matschei, B. Lothenbach, F.P. Glasser, The role of calcium carbonate in cement hydration, Cem. Concr. Res. 37 (2007) 551–558, https://doi.org/10.1016/j.cemconres.2006.10.013.

[20] M. Balonis, F.P. Glasser, The density of cement phases, Cem. Concr. Res. 39 (2009) 733–739, https://doi.org/10.1016/j.cemconres.2009.06.005.

[21] T. Oey, A. Kumar, J.W. Bullard, N. Neithalath, G. Sant, The filler effect: the influence of filler content and surface area on cementitious reaction rates, J. Am. Ceram. Soc. 96 (2013) 1978–1990, https://doi.org/10.1111/jace.12264.

[22] S. Sui, F. Georget, H. Maraghechi, W. Sun, K. Scrivener, Towards a generic approach to durability: factors affecting chloride transport in binary and ternary cementitious materials, Cem. Concr. Res. 124 (2019) 105783, , https://doi.org/10.1016/j.cemconres.2019.105783.

[23] Z. Yu, G. Ye, The pore structure of cement paste blended with fly ash, Constr. Build. Mater. 45 (2013) 30–35, https://doi.org/10.1016/j.conbuildmat.2013.04.012.

[24] E. Berodier, K. Scrivener, Evolution of pore structure in blended systems, Cem. Concr. Res. 73 (2015) 25–35, https://doi.org/10.1016/j.cemconres.2015.02.025.

[25] H. Maraghechi, F. Avet, H. Wong, H. Kamyab, K. Scrivener, Performance of Limestone Calcined Clay Cement (LC3) with various kaolinite contents with respect to chloride transport, Mater. Struct. 51 (2018) 125, https://doi.org/10.1617/s11527-018-1255-3.

[26] R.A. McKee, A generalization of the Nernst-Einstein equation for self-diffusion in high defect concentration solids, Solid State Lonics 5 (1981) 133–136.

[27] S.-Y. Hong, F.P. Glasser, Alkali binding in cement pastes, Cem. Concr. Res. 29 (1999) 1893–1903, https://doi.org/10.1016/S0008-8846(99)00187-8.

[28] K.B. Sanish, N. Neithalath, M. Santhanam, Monitoring the evolution of material structure in cement pastes and concretes using electrical property measurements, Constr. Build. Mater. 49 (2013) 288–297, https://doi.org/10.1016/j.conbuildmat.2013.08.038.

[29] FM5-578, Florida Method of Test for Concrete Resistivity as an Electrical Indicator of Its Permeability, (2004), pp. 4–7.

[30] Resipod,Proceq, http://Www.Proceq.Com/Fileadmin/Documents/Proceq/Products/Concrete/Resipod/English/Resipod_SF_E_2013.06.19_low.Pdf. (n.d.).

[31] N.T. Build 492, Concrete, mortar and cement-based repair materials: chloride migration coefficient from non-steady-state migration experiments, NordTest (1999) 1–8.

[32] ASTM-C1760, ASTM Standard C1760 - Standard Test Method for Bulk Electrical Conductivity of Hardened Concrete, i ASTM Int, 2012, pp. 1–5, https://doi.org/10.1520/C1760-12.2.

[33] Y. Bu, R. Spragg, W.J. Weiss, Comparison of the pore volume in concrete as determined using ASTM C642 and vacuum saturation, Adv. Civ. Eng. Mater. 3 (2014) 20130090, , https://doi.org/10.1520/ACEM20130090.

[34] AASHTO-PP84, Standard practice for developing performance engineered concrete pavement mixtures, Am. Assoc. State Highw. Transp. Off. 1 (2017) 1–36.

[35] G.E. Archie, The electrical resistivity log as an aid in determining some reservoir characteristics, Trans. AIME 146 (1942) 54–62, https://doi.org/10.2118/

942054-G.

[36] E.J. Garboczi, Permeability, diffusivity, and microstructural parameters: a critical review, Cem. Concr. Res. 20 (1990) 591–601.

[37] P. Yang, G. Sant, N. Neithalath, A refined, self-consistent Poisson-Nernst-Planck (PNP) model for electrically induced transport of multiple ionic species through concrete, Cem. Concr. Compos. 82 (2017) 80–94, https://doi.org/10.1016/j.cemconcomp.2017.05.015.

[38] R. Snellings, J. Chwast, Ö. Cizer, N. De Belie, Y. Dhandapani, P. Durdzinski, J. Elsen, J. Haufe, D. Hooton, C. Patapy, M. Santhanam, K. Scrivener, D. Snoeck, L. Steger, S. Tongbo, A. Vollpracht, F. Winnefeld, B. Lothenbach, TC 238-SCM: hydration stoppage methods for phase assemblage studies of blended cements – results of a round robin test, Mater. Struct. 51 (2018) 1–12, https://doi.org/10.1617/s11527-018-1237-5.

[39] R.S. Barneyback, S. Diamond, W. Lafayette, Expression and analysis of pore fluids from hardened cement pastes and mortars, Cem. Concr. Res. 11 (1981) 279–285.

[40] K.A. Snyder, X. Feng, B.D. Keen, T.O. Mason, Estimating the electrical conductivity of cement paste pore solutions from OH^-, K^+ and Na^+ concentrations, Cem. Concr. Res. 33 (2003) 793–798, https://doi.org/10.1016/S0008-8846(02)01068-2.

[41] T.C. Powers, Structure and physical properties of hardened Portland cement paste, J. Am. Ceram. Soc. 41 (1958) 1–6, https://doi.org/10.1111/j.1151-2916.1958.tb13494.x.

[42] M. Antoni, J. Rossen, F. Martirena, K. Scrivener, Cement substitution by a combination of metakaolin and limestone, Cem. Concr. Res. 42 (2012) 1579–1589, https://doi.org/10.1016/j.cemconres.2012.09.006.

[43] P. Mondai, S.R. Shah, L.D. Marks, Nanoscale characterization of cementitious materials, ACI Mater. J. 105 (2008) 174–179, https://doi.org/10.1002/adma.200802129.

[44] C. Andrade, V.M.M. Blanco, a Collazo, M. Keddam, X.R. No, H. Takenouti, X.R. Nóvoa, H. Takenouti, X.R. No, H. Takenouti, Cement paste hardening process studied by impedance spectroscopy, Electrochim. Acta 44 (1999) 4313–4318, https://doi.org/10.1016/S0013-4686(99)00147-4.

[45] Y. Dhandapani, K. Vignesh, T. Raja, M. Santhanam, Development of the microstructure in LC3 systems and its effect on concrete properties, Calcined Clays Sustain. Concr. Proc. 2nd Int. Conf. Calcined Clays Sustain. Concr, 2018, pp. 131–140, , https://doi.org/10.1007/978-94-024-1207-9_21.

[46] Y. Dhandapani, M. Santhanam, Characterisation of microstructure in limestone calcined clay cementitious systems, RILEM Spring Conv. Sustain. Mater. Syst. Struct. Conf. Rovinj, Croat. 18–22 March 2019, 2019.

[47] E. Gallucci, X. Zhang, K.L. Scrivener, Effect of temperature on the microstructure of calcium silicate hydrate (C-S-H), Cem. Concr. Res. 53 (2013) 185–195, https://doi.org/10.1016/j.cemconres.2013.06.008.

[48] ACI, 222R-01, Protection of Metals in Concrete against Corrosion, (2001).

[49] H. Muni, Y. Dhandapani, K. Vignesh, M. Santhanam, Anomalous early increase in concrete resistivity with calcined clay binders, Calcined Clays Sustain. Concr. Proc. 3nd Int. Conf. Calcined Clays Sustain. Concr, 2019, pp. 1–8.

[50] N.C.S.N. W, A. PP84, AASHTO-PP84, Standard practice for developing performance engineered concrete pavement mixtures standard practice for, Am. Assoc. State Highw. Transp. Off. 1 (2017) 1–36.

[51] International Federation for Structural Concrete, MC-SLD:2006. Model Code for Service Life Design (CEB-FIB Bulletin No. 34), 2006.

[52] V.J. Azad, D. Ph, A.R. Erbektas, A.M. Asce, C. Qiao, D. Ph, O.B. Isgor, D. Ph, W.J. Weiss, D. Ph, A.M. Asce, Relating the formation factor and chloride binding parameters to the apparent chloride diffusion coefficient of concrete, J. Mater. Civ. Eng. 31 (2019) 1–10, https://doi.org/10.1061/(ASCE)MT.1943-5533.0002615.

[53] A.T. Coyle, C. Qiao, A.T. Coyle, O.B. Isgor, W.J. Weiss, Prediction of chloride ingress in saturated concrete using formation factor and chloride binding isotherm concrete using formation factor and, Adv. Civ. Eng. Mater. 7 (2018) 206–220, https://doi.org/10.1520/ACEM20170141.

[54] O.B. Isgor, W.J. Weiss, A nearly self-sufficient framework for modelling reactive-transport processes in concrete, Mater. Struct. 52 (2019) 3, https://doi.org/10.1617/s11527-018-1305-x.

[55] C. Andrade, M. Castellote, R. D'Andrea, Measurement of ageing effect on chloride diffusion coefficients in cementitious matrices, J. Nucl. Mater. 412 (2011) 209–216, https://doi.org/10.1016/j.jnucmat.2010.12.236.

[56] K. Stanish, M. Thomas, The use of bulk diffusion test to establish time dependent concrete chloride diffusion coefficients, Cem. Concr. Res. 33 (2003) 55–62, https://doi.org/10.1016/S0008-8846(02)00925-0.

[57] M. Nokken, A. Boddy, R.D. Hooton, M.D.A. Thomas, Time dependent diffusion in concrete-three laboratory studies, Cem. Concr. Res. 36 (2006) 200–207, https://doi.org/10.1016/j.cemconres.2004.03.030.

[58] R.G. Pillai, R. Gettu, M. Santhanam, S. Rengaraju, Y. Dhandapani, S. Rathnarajan, A.S. Basavaraj, Service life and life cycle assessment of reinforced concrete systems with limestone calcined clay cement (LC3), Cem. Concr. Res. 118 (2019) 111–119, https://doi.org/10.1016/j.cemconres.2018.11.019.

[59] E. L'Hopital, B. Lothenbach, D.A. Kulik, K. Scrivener, Influence of calcium to silica ratio on aluminium uptake in calcium silicate hydrate, Cem. Concr. Res. 85 (2016) 111–121, https://doi.org/10.1016/j.cemconres.2016.01.014.

[60] E. L'Hôpital, B. Lothenbach, G. Le Saout, D. Kulik, K. Scrivener, Incorporation of aluminium in calcium-silicate-hydrates, Cem. Concr. Res. 75 (2015) 91–103, https://doi.org/10.1016/j.cemconres.2015.04.007.

[61] E. L'Hôpital, B. Lothenbach, K. Scrivener, D.A.A. Kulik, Alkali uptake in calcium alumina silicate hydrate (C-A-S-H), Cem. Concr. Res. 85 (2016) 122–136, https://doi.org/10.1016/j.cemconres.2016.03.009.

[62] Y. Bu, J. Weiss, The influence of alkali content on the electrical resistivity and transport properties of cementitious materials, Cem. Concr. Compos. 51 (2014) 49–58, https://doi.org/10.1016/j.cemconcomp.2014.02.008.

[63] H.M. Jennings, Model for the microstructure of calcium silicate hydrate in cement paste, Cem. Concr. Res. 30 (2000) 101–116, https://doi.org/10.1016/S0008-8846(99)00209-4.

[64] H.M. Jennings, J.J. Thomas, J.S. Gevrenov, G. Constantinides, F.J. Ulm, A multi-technique investigation of the nanoporosity of cement paste, Cem. Concr. Res. 37 (2007) 329–336, https://doi.org/10.1016/j.cemconres.2006.03.021.

[65] G. Constantinides, F.J. Ulm, The effect of two types of C-S-H on the elasticity of cement-based materials: results from nanoindentation and micromechanical modeling, Cem. Concr. Res. 34 (2004) 67–80, https://doi.org/10.1016/S0008-8846(03)00230-8.

[66] G. Constantinides, On the use of nanoindentation for cementitious materials, Mater. Struct. 36 (2003) 191–196, https://doi.org/10.1617/14020.

[67] G. Sant, D. Bentz, J. Weiss, Capillary porosity depercolation in cement-based materials: measurement techniques and factors which influence their interpretation, Cem. Concr. Res. 41 (2011) 854–864, https://doi.org/10.1016/j.cemconres.2011.04.006.

[68] L. Yuan-Hui, S. Gregory, Diffusion of ions in sea water and in deep-sea sediments, Geochim. Cosmochim. Acta 38 (1974) 703–714, https://doi.org/10.1016/0016-7037(74)90145-8.

[69] M. Ben Clennell, Tortuosity: a guide through the maze, Geol. Soc. London, Spec. Publ. 122 (1997) 299–344, https://doi.org/10.1144/GSL.SP.1997.122.01.18.

[70] R. Spragg, C. Qiao, T. Barrett, J. Weiss, W. Lafayette, T. Beijing, Assessing a concrete's resistance to chloride ion ingress using the formation factor, Corros. Steel Concr. Struct. (2016) 211–236.

[71] A. Poshnath, Investigation of Time Dependency in Chloride Transport Parameters for Service Life Estimation of Blended Cementitious Systems, Master's Thesis IIT Madras, 2019.

[72] P.T. Durdziński, M. Ben Haha, M. Zajac, K.L. Scrivener, Phase assemblage of composite cements, Cem. Concr. Res. 99 (2017) 172–182, https://doi.org/10.1016/j.cemconres.2017.05.009.

[73] K. Scrivener, A. Ouzia, P. Juilland, A. Kunhi Mohamed, Advances in understanding cement hydration mechanisms, Cem. Concr. Res. 124 (2019) 105823, , https://doi.org/10.1016/j.cemconres.2019.105823.

[74] J. Skibsted, R. Snellings, Reactivity of supplementary cementitious materials (SCMs) in cement blends, Cem. Concr. Res. 124 (2019) 105799, , https://doi.org/10.1016/j.cemconres.2019.105799.